Prolonged Metamorphism During Long-Lived Terrane Accretion: Sm-Nd Garnet and U-Pb Zircon Geochronology and Pressure-Temperature Paths from the Salmon River Suture Zone, West-Central Idaho, USA

Matthew P. McKay – University of Vermont
Elizabeth M. Bollen – University of Alabama
Keith D. Gray – Wichita State University
Harold Stowell – University of Alabama
Joshua Schwartz – California State University

Citation of published version:
McKay, M., Bollen, E., Gray, K., Stowell, H., Schwartz, J. (2017): Prolonged Metamorphism During Long-Lived Terrane Accretion: Sm-Nd Garnet and U-Pb Zircon Geochronology and Pressure-Temperature Paths from the Salmon River Suture Zone, West-Central Idaho, USA. *Lithosphere*, 9(5).
Direct Link to Article:
https://pubs.geoscienceworld.org/gsa/lithosphere/article/9/5/683/208083/prolonged-metamorphism-during-long-lived-terrane

THE GEOLOGICAL SOCIETY OF AMERICA®

Prolonged metamorphism during long-lived terrane accretion: Sm-Nd garnet and U-Pb zircon geochronology and pressure-temperature paths from the Salmon River suture zone, west-central Idaho, USA

Matthew P. McKay[1], Elizabeth M. Bollen[2], Keith D. Gray[3], Harold H. Stowell[2], and Joshua J. Schwartz[4]
[1]DEPARTMENT OF GEOGRAPHY, GEOLOGY AND PLANNING, MISSOURI STATE UNIVERSITY, 901 S. NATIONAL AVENUE, SPRINGFIELD, MISSOURI 65897, USA
[2]DEPARTMENT OF GEOLOGICAL SCIENCES, UNIVERSITY OF ALABAMA, 2003 BEVILL BUILDING, TUSCALOOSA, ALABAMA 35487, USA
[3]DEPARTMENT OF GEOLOGY, WICHITA STATE UNIVERSITY, GEOLOGY BUILDING, 1845 FAIRMOUNT STREET, WICHITA, KANSAS 67260, USA
[4]DEPARTMENT OF GEOLOGICAL SCIENCES, CALIFORNIA STATE UNIVERSITY, NORTHRIDGE, LIVE OAK 1202, 18111 NORDHOFF STREET, NORTHRIDGE, CALIFORNIA 91330, USA

ABSTRACT

The Salmon River suture zone of western Idaho (USA) records mid-crustal metamorphism and deformation associated with orogenesis during Mesozoic accretion of volcanic arc terranes to western Laurentia. We present petrographic and microstructural observations, garnet geochemistry, pressure-temperature isochemical phase diagrams, and Sm-Nd garnet and U-Pb zircon ages to investigate the timing and conditions of metamorphism in the Salmon River suture zone. The Salmon River suture zone is comprised of three thrust sheets: from east to west, the amphibolite facies Pollock Mountain plate, upper greenschist to amphibolite facies Rapid River plate, and greenschist facies Heavens Gate plate. The Pollock Mountain plate was isothermally loaded from 6 to >8 kbar at ~700 °C between 141 and 124 Ma during northwest-southeast crustal shortening. The underlying Rapid River plate was isothermally loaded from 7 to ~10 kbar at 600–650 °C during ca. 124–112 Ma metamorphism, which is contemporaneous with late- to post-peak metamorphism and ca. 118 Ma exhumation of the overlying Pollock Mountain plate. In the Rapid River plate, thrust sheet emplacement induced high-strain ductile deformation and led to regional development of linear-planar fabrics. The $^{206}Pb/^{238}U$ zircon ages for syndeformational to postdeformational magmatism record ca. 117 Ma or younger juxtaposition of the two plates on the southeast-dipping Pollock Mountain thrust fault. Coeval 124–112 Ma metamorphism of the Rapid River plate, ca. 118 Ma exhumation of the Pollock Mountain plate, and ca. 117 Ma or younger movement along the Pollock Mountain fault suggest that metamorphism of the Rapid River plate was possibly driven in part by thrust juxtaposition and loading along the Pollock Mountain fault. In this context, we interpret that metamorphism records diachronous thrust stacking during prolonged (>30 m.y.) accretionary orogenesis in western Idaho.

LITHOSPHERE; v. 9; no. 5; p. 683–701; GSA Data Repository Item 2017234 | Published online 30 June 2017 doi:10.1130/L642.1

INTRODUCTION

Continental assembly and crustal growth along active margins are dominated by accretion of allochthonous terranes and magmatic additions from the underlying mantle (e.g., Coney et al., 1980; Scholl et al., 1986). The collision of displaced terranes with cratonic margins is often accompanied by contractional deformation and crustal thickening, which generally leads to anatexis and regional metamorphism (Chamberlain and Karabinos, 1987). The age and pressure-temperature (*P-T*) conditions during metamorphism in the roots of arc-continent collision zones are critical for understanding collisional processes including the time scales and mechanisms of thermal perturbations, the extent and driving forces behind the metamorphism and partial melting, and the magnitude and timing of deformation in the middle to lower crust. In orogenic belts where laterally extensive tracts of deep-crustal rocks are exposed (e.g., Western Gneiss region of Norway and Pamir Plateau of Central Asia), metamorphic and thermochronologic studies indicate that widespread chemical and thermal equilibrium is not uniformly achieved during collisional orogenesis (Spencer et al., 2013; Stearns et al., 2015). Determining the age of metamorphism and conditions during synmetamorphic deformation provide crucial insight into the tectonic processes at work. In this study we present Sm-Nd garnet and U-Pb zircon ages along with integrated isochemical phase diagram models and thermobarometry estimates to construct *P-T*-time paths that reflect the evolution of orogenic belts roots through time.

The Salmon River suture zone of western Idaho (USA) exposes mid-crustal rocks across a complex island arc–continent collision zone and provides an ideal opportunity to resolve the duration, magnitude (i.e., *P-T* conditions through time), and spatial patterns of metamorphism during accretionary orogenesis. The Salmon River suture zone is located in the central North American Cordillera, and is dominated by metasedimentary and metavolcanic rocks of island arc affinity that record progressive deformation and metamorphism during Late Jurassic to Early Cretaceous accretion of the Blue Mountains province to western Laurentia (Fig. 1; Silberling et al., 1984; Lund and Snee, 1988; Avé Lallemant, 1995; Snee

Matthew McKay http://orcid.org/0000-0002-7756-6489

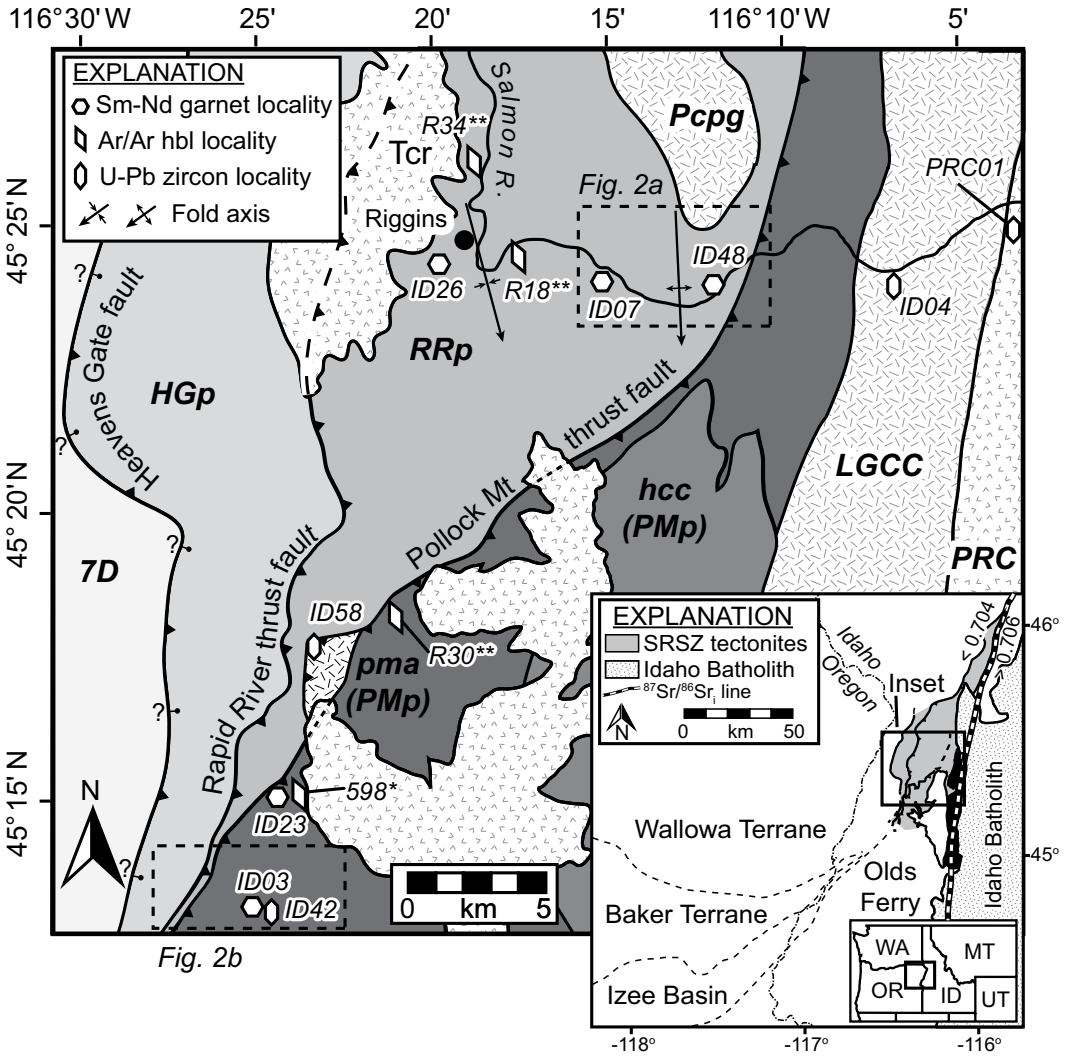

Figure 1. Geologic map of the Salmon River suture zone (SRSZ). 7D—Seven Devils volcanics of Wallowa terrane; HGp—Heavens Gate plate; RRp—Rapid River plate; PMp—Pollock Mountain plate; Kh—Hazard Creek Complex; LGCC—Little Goose Creek Complex; Tcr—Columbia River Basalt Group; Pcp—Permian Chair Point pluton. Fold symbols mark the axes of the Riggins synform and Lake Creek antiform (after Hamilton, 1969; Lund, 2004; Gray, 2013). Locations of Figures 2A and 2B are shown. Sample localities from this study (ID03, ID07, ID23, ID26, ID48) and previously published geochronology and thermochronology results (* denotes $^{40}Ar/^{39}Ar$ hornblende ages from Getty et al., 1993; ** denotes $^{40}Ar/^{39}Ar$ hornblende ages from Lund and Snee, 1988; 598—119 ± 2 Ma; R18—106.5 ± 1.4 Ma; R30—118.0 ± 0.6 Ma; R34 = 109.1 ± 0.6 Ma).

et al., 1995; Wyld and Wright, 2001; Wyld et al., 2006; Blake et al., 2009; Gray et al., 2012). Historically, the Salmon River suture zone has played a fundamental role in tectonic models describing the evolution of the central North American Cordillera (Oldow et al., 1989; Burchfield et al., 1992; McClelland et al., 2000; Wyld and Wright, 2001; Giorgis et al., 2005). Early studies postulated that metamorphism in the suture zone (Hamilton, 1963; Onasch, 1977) was related to intrusion of the 100–54 Ma Idaho batholith (Gaschnig et al., 2010) to the east. More recent tectonic models incorporating Sm-Nd garnet geochronology have proposed that island arc amalgamation and subsequent accretion were recorded by distinct metamorphic events that occurred ca. 144 Ma and ca. 128 Ma (Selverstone et al., 1992; Getty et al., 1993).

One problem associated with garnet age interpretation is that isotopic measurements typically require large sample masses to achieve high precision, introducing the possibility that isotopic garnet analyses may reflect a mixed value between two different age domains within a single crystal, and fail to resolve long-duration garnet growth. Complicated zoning, particularly in polymetamorphic garnet (e.g., Stowell and Goldberg, 1997), adds complexity because precise ages for each event requires sampling separate zones for individual isotope analyses. In addition, the possible adverse effects of inclusions must be considered (e.g., Prince et al., 2000). The resulting lack of age resolution presents problems in relating garnet growth to discrete tectonothermal events. In this study we have attempted to minimize the impacts of age mixing by microsampling distinct chemical and textural zones within garnet from amphibolites. We combine new Sm-Nd garnet ages with additional geochronologic data (U-Pb zircon, Ar-Ar hornblende), *P-T* estimates, and fabric element analyses (microscopic to map scale) to provide insights into the processes of regional metamorphism and deformation associated with arc-continent collision during protracted subduction-driven orogeny (Selverstone et al., 1992). Based on these new data, we present a tectonic model for the Salmon River suture zone, wherein long-lived regional metamorphism is controlled by diachronous thrust stacking. In this model, protracted metamorphism and contractional deformation occurred over a period of 30 m.y. or more, during which the Blue Mountains province was incorporated into the Laurentian margin.

GEOLOGIC BACKGROUND

Blue Mountains Province

The North American Cordillera largely consists of an assemblage of terranes that were progressively accreted to western Laurentia during Phanerozoic subduction of the Farallon plate (Coney et al., 1980; Engebretson

et al., 1985). In west-central Idaho, the initial $^{87}Sr/^{86}Sr = 0.706$ isopleth is subparallel to longitude ~116°W and marks the geochemical boundary between rocks with cratonic affinity to the east and accreted terranes to the west (Armstrong et al., 1977; Fleck and Criss, 2004) (Fig. 1). This isotopic boundary is within the Salmon River suture zone and defines the eastern edge of the Blue Mountains province (Silberling et al., 1984, 1987). The Blue Mountains province is comprised of four terranes (Olds Ferry, Baker, Izee, and Wallowa) that record late Paleozoic to Mesozoic magmatism, metamorphism, and sedimentation within two volcanic arc systems (e.g., Dickinson, 1979; Walker, 1986; Vallier, 1977, 1995; Schwartz et al., 2010).

The Wallowa (Permian–Jurassic) and Olds Ferry (Triassic–Jurassic) terranes are subduction-related volcanic arc systems (Vallier, 1995; Avé Lallemant, 1995; Kurz et al., 2012). The Wallowa arc formed at a distal location (~18° north of the paleoequator; Hillhouse et al., 1982), whereas the Olds Ferry fringing arc was constructed along the Laurentian margin similar to the modern-day Aleutian volcanic arc (Vallier, 1995). In Avé Lallemant (1995) and Schwartz et al. (2010, 2011), it was proposed that the Baker terrane represents the accretionary complex and forearc components of the Olds Ferry island arc. This model is supported by structural and isotopic (Rb-Sr, Sm-Nd) data and similarities in detrital zircon age populations between the Baker and Olds Ferry terranes (Alexander and Schwartz, 2009; Schwartz et al., 2010, 2011). The Wallowa and Olds Ferry terranes were amalgamated offshore during Late Jurassic time, as recorded by ca. 159–154 Ma contractional deformation along this terrane boundary (Schwartz et al., 2010, 2011). Structural studies along the Wallowa-Baker terrane boundary document the development of northward-directed thrust faults and east-west folds associated with imbrication of the Wallowa arc (Schwartz et al., 2010). Deformation occurred at upper greenschist to lower amphibolite facies conditions (Ferns and Brooks, 1995; Schwartz et al., 2010). The Blue Mountains province obtained its current position (Fig. 1 inset) after collision with the Laurentian margin (Engebretson et al., 1985; Giorgis et al., 2008) and clockwise oroclinal rotation beginning ca. 126 Ma (Wilson and Cox, 1980; Žák et al., 2015). Accretion of the Wallowa terrane was proposed to have occurred during the Early to Middle Jurassic (LaMaskin et al., 2015). The lack of craton-derived Precambrian or Paleozoic detrital zircon populations in marine strata of the Wallowa terrane (Jurassic Coon Hollow Formation; LaMaskin et al., 2015) and ages of deformation in the Blue Mountains region, however, suggest Late Jurassic to Early Cretaceous initiation of arc-continent collision (Lund and Snee, 1988; Avé Lallemant, 1995; Blake et al., 2009; Schwartz et al., 2010, 2011, 2014; Gray et al., 2012; Žák et al., 2015).

Salmon River Suture Zone

Western portions of the Salmon River suture zone consist of greenschist to upper amphibolite facies metamorphic rocks that are directly west of the initial $^{87}Sr/^{86}Sr = 0.706$ isopleth (Fig. 1). The north- to northeast-striking Salmon River suture zone is oriented subparallel to internal terrane boundaries of the Blue Mountains province that appear to converge ~100 km southwest of Riggins, Idaho (Fig. 1 inset). Near Riggins, Idaho, the suture zone is bound to the east by undeformed and unmetamorphosed granitic rocks of the Idaho batholith (Taubeneck, 1971; Gaschnig et al., 2010) and to the west by the east- to southeast-dipping Heavens Gate fault (Fig. 1), which carries greenschist tectonites in the hanging wall over lower grade volcanic rocks of the Wallowa terrane (Gray and Oldow, 2005; Gray, 2013). In this study, L-S tectonites between the Heavens Gate fault and initial Sr 0.706 isopleth are divided into three structural plates separated by the Pollock Mountain thrust fault (Aliberti, 1988) and the Rapid River thrust fault (Hamilton, 1963): from east to west, these are the Pollock Mountain, Rapid River, and Heavens Gate plates (Fig. 1).

The structurally highest Pollock Mountain plate includes medium- to high-grade gneissic amphibolite and orthogneiss (Figs. 2A–2C) (Pollock Mountain amphibolite of Aliberti, 1988) and overlies the Rapid River plate across the southeast-dipping Pollock Mountain thrust fault. Metamorphic rocks in this plate were intruded by the Hazard Creek Complex between ca. 118 and 114 Ma (U-Pb zircon; Manduca et al., 1993; Unruh et al., 2008) (Figs. 1 and 2B). Peak metamorphic conditions in the Pollock Mountain plate are estimated as 8–11 kbar and 600–625 °C (Selverstone et al., 1992), and are inferred to predate emplacement of the syntectonic, epidote-bearing Hazard Creek Complex (Manduca et al., 1993; Fleck and Criss, 2004). A hornblende $^{40}Ar/^{39}Ar$ age of 119 ± 2 Ma from the Pollock Mountain amphibolite (Getty et al., 1993) indicates that the thrust sheet cooled below the closure temperature of Ar in hornblende (~525 °C) during emplacement of the Hazard Creek Complex.

The underlying Rapid River plate contains Riggins Group sedimentary and volcanic rocks that were metamorphosed at upper greenschist to amphibolite facies, with metamorphic grade increasing toward the east (Hamilton, 1960, 1963, 1969). Metasedimentary rocks of the Riggins Group have been correlated with volcaniclastic and sedimentary units of the Wallowa terrane (Seven Devils Group of Vallier, 1977; Lund, 1984; Lund et al., 1993; Kauffman et al., 2014; Schmidt et al., 2016), Huntington Formation of the Olds Ferry terrane (Brooks and Vallier, 1978; Vallier, 1995), Baker terrane (Vallier, 1977; Brooks and Vallier, 1978), or Weatherby Formation of the Izee intra-arc basin (Brooks and Vallier, 1978; Dorsey and LaMaskin, 2007). The Rapid River plate is bound to the west by the Rapid River thrust system, which in our study area carries metamorphic tectonites of the Riggins Group over penetratively deformed Late Triassic carbonate rocks correlated with the Martin Bridge Formation (e.g., Hamilton, 1969; Onasch, 1977, 1987; Aliberti, 1988; Schmidt et al., 2016).

The lowest structural sheet of the Salmon River suture zone, the Heavens Gate plate, contains penetratively deformed metavolcanogenic, carbonate, and minor siliciclastic rocks that have been metamorphosed to upper greenschist facies and correlate with Middle to Late Triassic rocks in the Wallowa terrane (Wild Sheep Creek Formation; T.L. Vallier, 2012, personal commun.; Gray, 2013; Kauffman et al., 2014) (Fig. 1). In the northeastern Seven Devils Mountains (Heavens Gate Ridge), linear-planar tectonite fabrics structurally overlie massive volcanic flows of the Wild Sheep Creek Formation (Vallier, 1977, 1998) across the Heavens Gate fault.

Structural fabrics across the Salmon River suture zone include a north-striking, variably dipping, synmetamorphic foliation (S_1; regional schistosity; Onasch, 1987; Gray et al., 2012; Gray, 2013) defined by aligned phyllosilicate minerals (prochlorite ± muscovite ± biotite), flattened lithic clasts, or compositional banding (intrusive rocks). Primary igneous and sedimentary textures are locally preserved in rocks of low metamorphic grade, but are obscured by metamorphism and mylonitization in many areas. Analysis of triaxially deformed volcanic and carbonate clasts indicates that arc-supracrustal rocks primarily underwent a flattening strain (Hamilton, 1963; Aliberti, 1988), consistent with strain calculations in granitic rocks exposed >20 km to the east along the arc-continent boundary (Giorgis and Tikoff, 2004; Blake et al., 2009). Pervasive downdip to steeply pitching mineral or lithic clast stretching lineations (L_1) are typically well developed on S_1. East of the Heavens Gate fault, tectonite fabrics are deformed in upright, open to closed, postmetamorphic mesoscale to map-scale folds (e.g., Riggins synform, Lake Creek antiform; Fig. 1) that plunge shallowly to moderately southeast (Hamilton, 1963; Onasch, 1977; Blake, 1991; Bruce, 1998; Fig. 3).

According to Giorgis et al. (2005, 2008), accretion-related contractional structures (thrust faults, folds, and tectonite fabrics) of the Salmon River suture zone are overprinted by the mid-Cretaceous western Idaho

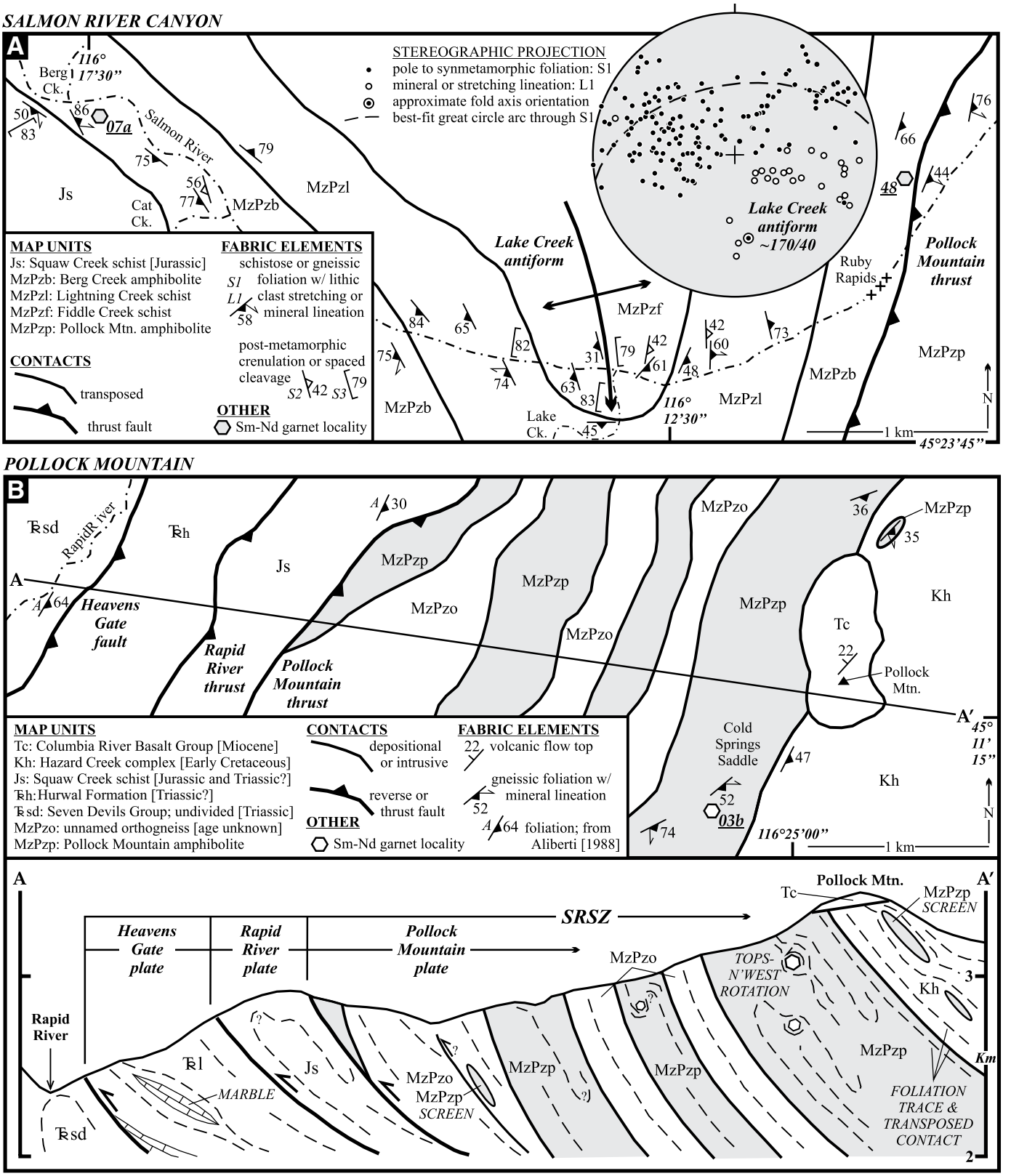

Figure 2. Simplified strip maps and structural section through areas sampled for Sm-Nd garnet geochronology; map locations are shown in Figure 1. (A) Salmon River canyon; sample localities ID07, ID48. Inset: Equal area stereographic projection plot highlights synmetamorphic fabric (S_1-L_1) folded by the upright, symmetric, southeast-plunging Lake Creek antiform (e.g., Onasch, 1977) (modified from Hamilton, 1969; Blake, 1991; Gray, 2013). (B) Pollock Mountain; sample locality ID03 (422 of Getty et al., 1993). Section A–A′ crosses the Pollock Mountain, Rapid River, and Heavens Gate thrust plates, i.e., accretion-related contractional structures of the Salmon River suture zone (SRSZ) (modified from Aliberti, 1988).

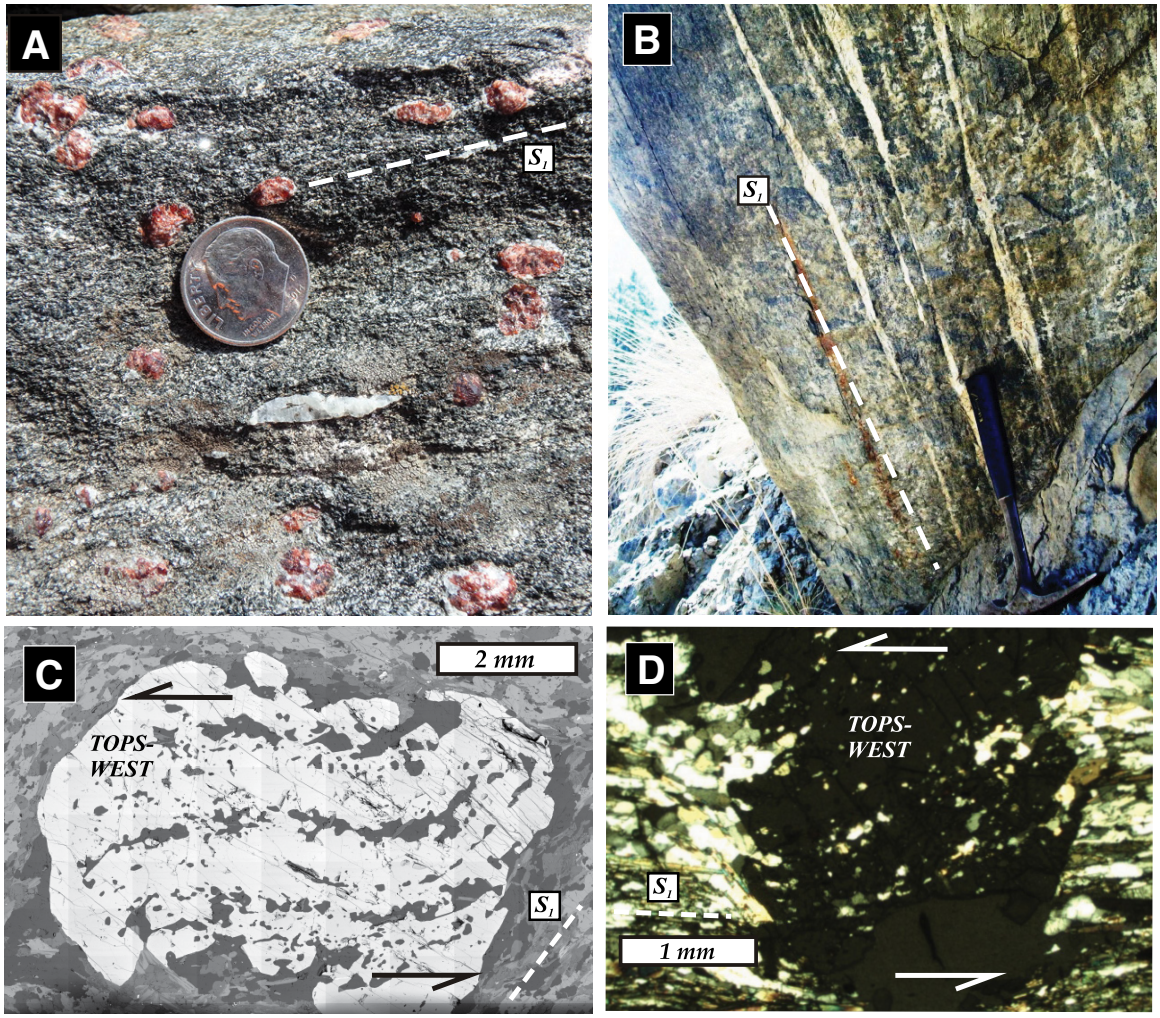

Figure 3. (A) Pollock Mountain Amphibolite exposed on Cold Springs Saddle, sample locality 03 (see map in Fig. 2B). Synmetamorphic foliation (S1) dips moderately southeast; trace of S_1 is indicated by dashed white line. Coin (17.9 mm diameter) is in the Y-Z strain plane, perpendicular to foliation. Note oblate (flattened) garnet porphyroblasts with long axes (Y) subparallel to foliation trace. View is to the southeast. (B) Berg Creek Amphibolite exposed in the Salmon River canyon; sample locality 07a (see map in Fig. 2A). Symmetrically deformed feldspar stringers reside in the X-Y strain plane, parallel to S1 (trace indicated by dashed line). View is to the southeast (foliation dips steeply southwest). Hammer for scale. (C) Backscatter electron image of garnet porphyroblast (locality 03) containing a sigmoidal inclusion trail pattern. In lower right, trails are parallel to the trace of S1 (dashed line). Note the termination of inclusion trails in lower left that project through rim overgrowth into alignment with matrix fabric. Inclusion trail patterns suggest top-to-the-northwest rotation. (D) Poikiloblastic garnet (locality 07a) showing moderately inclined trails extending into and merging with the trace of S_1 (dashed line). Inclusion trail patterns suggest top-to-the-west rotation. Thin section is cut perpendicular to foliation and parallel to amphibole lineation (L_1).

shear zone (McClelland et al., 2000; Tikoff et al., 2001). This north-south–striking shear zone is largely contained within eastern areas of the Salmon River suture zone and the Little Goose Creek Complex (Giorgis et al., 2008) and postdates collision of the Blue Mountains province with western Laurentia. It is unclear, however, whether the Salmon River suture zone and western Idaho shear zone are distinct tectonic elements that overlap or if they represent a single protracted orogen (McClelland et al., 2000; Giorgis et al., 2008; Gray et al., 2012). In either case, ductile deformation attributed to the western Idaho shear zone was active between ca. 120 and 90 Ma (Manduca et al., 1993; McClelland and Oldow, 2007; Giorgis et al., 2008); peak metamorphism occurred ca. 98 Ma (Braudy et al., 2017).

Getty et al. (1993) used Sm-Nd garnet geochronology and $^{40}Ar/^{39}Ar$ thermochronology to date metamorphism and cooling in the Pollock Mountain plate; they inferred that pre–144 Ma metamorphism corresponded to outboard collision of the Olds Ferry and Wallowa magmatic arcs and that overprinting ca. 128 Ma metamorphism dated docking of the Blue Mountains province to the Laurentian margin. The interpretation for pre–144 Ma terrane amalgamation is compatible with 159–154 Ma age constraints derived from Late Jurassic deformed sedimentary rocks and postkinematic stitching plutons within the Baker terrane (Schwartz et al., 2011). Getty et al. (1993) inferred that youngest garnet in the Salmon River suture zone grew during post-peak metamorphic cooling, as evidenced by garnet rim temperature estimates that record lower temperatures than garnet cores. Postmetamorphic cooling was documented by ca. 119 Ma hornblende $^{40}Ar/^{39}Ar$ ages in the Pollock Mountain plate (Lund and Snee, 1988; Getty et al., 1993) and ca. 118 Ma to ca. 101 Ma

(Lund and Snee, 1988; Snee et al., 1995) ages in the Rapid River plate. Garnet growth during cooling was inferred to occur during rapid tectonic exhumation during lithospheric delamination (Selverstone et al., 1992).

MICROSTRUCTURES AND MINERAL COMPOSITIONS

Field Sampling Localities

Garnet-bearing metamorphic tectonites at 5 localities (Figs. 1 and 2) were selected from more than 50 field locations (see McKay, 2011; Bollen, 2015; Table DR1[1]) for petrographic and structural analysis, whole-rock and garnet compositional analyses, and garnet Sm-Nd geochronology. Samples ID03 and ID23 are from the Pollock Mountain plate (Aliberti, 1988) and samples ID07 and ID26 are from the Rapid River plate (Berg Creek Amphibolite and Squaw Creek Schist of Hamilton, 1963). Sample ID48 was collected near the Pollock Mountain thrust fault, as depicted by Lund (2004) and described by Hamilton (1969, plate 1) as a "gradational change between arbitrarily designated units." Based on the biotite-rich schistose lithology, and similarity to pelitic rocks of the Rapid River plate, we place ID48 below the Pollock Mountain thrust and thus interpret it as part of the Rapid River plate. The locations for Pollock Mountain plate samples ID03 and ID23 correspond to locations 422 and 598 reported in Selverstone et al. (1992) and Getty et al. (1993). Rapid River plate samples (ID07, ID48) were selected based on (1) the presence of large (>3 mm), subhedral to euhedral garnet to permit Sm-Nd geochronology, and (2) distinct mineral assemblages (i.e., presence of zoisite and/or aluminum silicate) to improve *P-T* estimates.

Four U-Pb zircon geochronology samples were collected, two from the Pollock Mountain plate and two from the adjacent igneous complexes. Sample ID42 was collected from an orthogneiss located ~100 m southeast of sample ID03 within the Pollock Mountain plate. Sample ID58 is a heavily deformed orthogneiss that is cut by the Pollock Mountain thrust fault to the north and west, as mapped by Lund (2004). The ID58 sample locality is within the hanging wall of the Pollock Mountain thrust fault in the Pollock Mountain plate and inferred to have been emplaced during or just prior to thrusting of the Pollock Mountain thrust fault. Samples PRC01 and ID04 were collected from along the Salmon River within the Payette River complex and Little Goose Creek Complex, respectively.

Petrographic and Structural Analysis Methods

Structural fabrics at each sample locality were plotted on 1:24,000-scale geologic maps modified from Aliberti (1988) and Blake (1991) (Fig. 2). Geologic maps covering larger tracts of west-central Idaho (1:125,000 scale: Hamilton, 1969; 1:100,000 scale: Lund, 2004) were utilized to place local structures (Figs. 2 and 3) into a regional tectonic framework. Field observations were combined with microstructural analysis of oriented samples in an attempt to elucidate the timing relationships between garnet growth and fabric development. Oriented thin section slides were prepared at Washington State University, and backscattered electron (BSE) images were collected at the University of Alabama.

Mineral Analysis

Quantitative and qualitative mineral compositions were determined on the JEOL 8600 electron probe microanalyzer at the University of Alabama Central Analytical Facility. Quantitative analyses of garnet, hornblende, plagioclase, and biotite were obtained using wavelength dispersive spectrometry with a 1–5 μm beam diameter, 30–45 s count times, under a 20 nA beam at 15 kV for point and line scan analyses. Synthetic compound and mineral standards were used to convert raw counts to weight percent oxide using the CitZAF correction method (Armstrong, 1984). X-ray K-α intensity maps and BSE images were collected with 20–50 nA beam current and 15 kV using 5–7 s count times. Analytical traverses or line scans across mineral grains were collected to document the zoning of garnet. Inclusions in garnet that were incidentally analyzed were excluded from line scans by identifying non-garnet analyses using mineral stoichiometry (±0.02). Garnet line scans plotted in Figures 4 and 5 are in mole proportions.

Pollock Mountain Plate

Petrography: ID03

Ridgeline exposures west of Pollock Mountain (e.g., Cold Springs Saddle) form part of a steeply southeast-dipping sequence of alternating garnet-biotite-plagioclase-hornblende amphibolite and felsic hornblende-biotite orthogneiss (Aliberti, 1988). This sequence occupies the hanging wall of the northeast-striking Pollock Mountain thrust fault, which lies ~2.5 km west of our sample locality ID03 (Fig. 2B). In this area, the fault intersects ridge and valley topography at a high angle (60°–90°), indicating a steep to moderate southeast-dipping structure.

Sample ID03 is an amphibolite containing garnet, hornblende, biotite, plagioclase, quartz, ilmenite, and rutile. Subhedral, medium- to coarse-grained (5–15 mm) garnet porphyroblasts locally characterize this unit within the Pollock Mountain amphibolite (Fig. 3A). The garnet mode is ~7%. Inclusions in garnet of hornblende, plagioclase, quartz, and ilmenite form well-developed trails through subhedral cores of two-stage garnet porphyroblasts (Figs. 3C and 4B), which are overgrown by narrow, 1–2 mm, inclusion-free rims. Rotated inclusion patterns (Williams and Jiang, 1999) preserved in cores (stage I) suggest top-to-the-northwest shear, consistent with kinematic indicators in single-stage garnet of the Salmon River canyon (ID07; Fig. 2A). Some garnet grains contain semicontinuous inclusion trails that are oriented subparallel to external matrix fabric; however, trail patterns typically terminate along core margins where rim overgrowths (stage II) are encountered. Garnet grains are partially wrapped by a strong southeast-dipping gneissic foliation defined by millimeter-scale hornblende, biotite, and plagioclase layers; aligned hornblende grains form a moderately developed east- to southeast-plunging mineral lineation. Synmetamorphic foliation at locality ID03 is subparallel to pervasive gneissic fabrics in adjacent rocks of the Hazard Creek Complex (Manduca et al., 1993) exposed east of Pollock Mountain (e.g., Aliberti, 1988; Fig. 2B). The composition of garnet grains (Figs. 4A, 4B) records end-member zoning across both garnet cores and narrow, inclusion-free rims. Spessartine content decreases and Mg# increases from the core outward, interpreted here to indicate prograde growth (Fig. 4A). Almandine content shows subtle variation and increases slightly toward the rim. Grossular and pyrope increase slightly toward the rim. The core-rim boundary does not show a sharp compositional break; however, there is a slight decrease in almandine. Increases in grossular and almandine and a decrease in pyrope within 1 mm of the left side of the line scan may reflect diffusion. This diffusion is not obvious on the right side of the line scan.

Petrography: ID23

Sample ID23 is a schist containing garnet, staurolite, kyanite, biotite, plagioclase, quartz, rutile, and ilmenite collected 5.6 km northeast from sample ID03. The sample is characterized by subhedral garnet porphyroblasts ≥8 mm in diameter containing staurolite, biotite, ilmenite, rutile, plagioclase, and quartz inclusions (Fig. 4D). The garnet mode is ~10%.

[1]GSA Data Repository Item 2017234, Whole rock and mineral geochemistry, garnet and zircon isotope geochronology data, and methods, is available at http://www.geosociety.org/datarepository/2017, or on request from editing@geosociety.org.

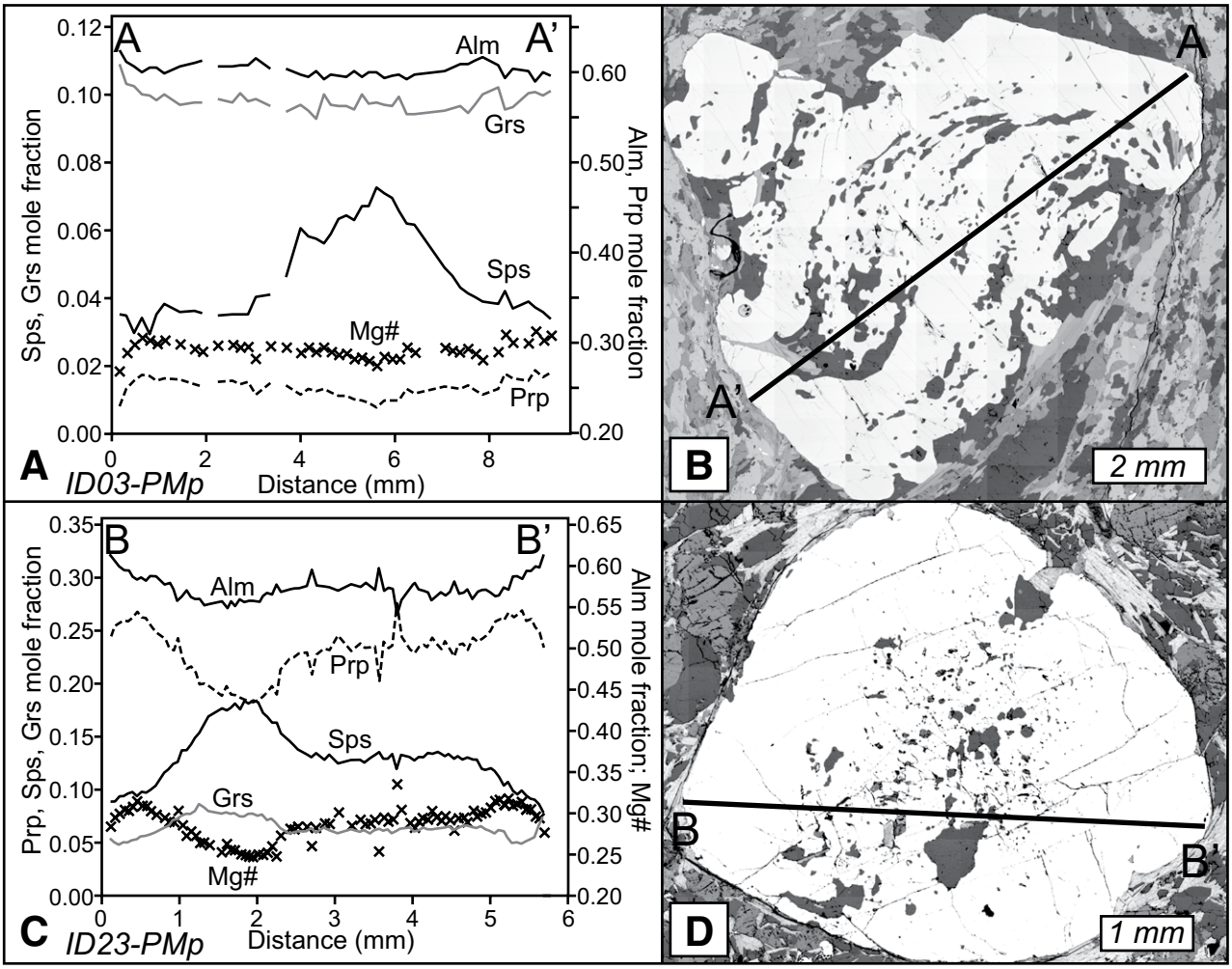

Figure 4. Pollock Mountain garnet compositions from rim to rim along lines shown in the backscatter electron (BSE) images. Garnets have spessartine-rich, inclusion-rich cores encased in lower spessartine, inclusion-poor rims. PMp—Pollock Mountain plate; Alm—almandine; Grs—grossular; Prp—pyrope; Sps—spessartine. (A) ID03 line scan (n = 46). (B) ID03 (BSE). (C) ID23 line scan (n = 87). (D) ID23 (BSE).

Ilmenite inclusions are restricted to garnet cores, whereas rutile occurs within garnet rims and matrix. Quartz inclusion trails observed in garnet cores are oblique to external matrix fabric. Garnet compositional line scans (Figs. 4C, 4D) show strong zoning patterns in all end members. The compositional center appears offset from the geometric center of the crystal, possibly due to late-stage resorption or missing the actual core in the third dimension. The compositional center corresponds with the inclusion-rich core. Spessartine decreases and Mg# increases outward from the core toward the rim, indicating prograde growth. Almandine and pyrope steadily increase toward the rim and grossular decreases. The inclusion-rich core contains higher spessartine, grossular, pyrope, and lower almandine than the rim. Diffusion likely affected the outer 0.5 mm rim of the garnet in a narrow zone where almandine and grossular increase, and spessartine and pyrope decrease.

Rapid River Plate

Petrography: ID07

Along the steep western limb of the Lake Creek antiform (Fig. 2A), inclusion-rich garnet porphyroblasts overgrow and are partially wrapped by northwest-striking synmetamorphic foliation (S_1) in the Berg Creek Amphibolite (Fig. 3B). Sample ID07, collected from this area, is an amphibolite containing garnet, hornblende, zoisite, clinozoisite, plagioclase, quartz, ilmenite, and rutile. This sample contains medium-grained (1–5 mm), highly fractured, subhedral garnet and aggregate clusters elongated parallel to the trace of S_1. The garnet mode is ~6%. Garnets contain evenly distributed mineral inclusions of clinozoisite, quartz, plagioclase, and rutile, which form linear to weakly sigmoidal patterns that appear to merge with the trace of S_1 (Fig. 3D). Inclusion trails oblique to S_1 suggest that some grains underwent ~45° counterclockwise (top to the southwest) rotational strain with respect to enclosing fabric. Microfractures are generally oriented perpendicular to S_1, which is defined here by millimeter-scale layering composed of plagioclase, quartz, hornblende, zoisite, ± calcite in a ferromagnesian sedimentary or volcanic protolith (Hamilton, 1963; Bruce, 1998). Southeast-plunging mineral lineations (L_1) formed by aligned hornblende are moderately developed on S_1 (Blake et al., 2009, 2016).

Garnet compositional zoning from ID07 shows subtle, simple zoning in all end members (Fig. 5A). Spessartine, pyrope, and Mg# decrease and grossular increases toward the rim. Almandine shows very little zoning. The decrease in spessartine from core to rim is best interpreted as

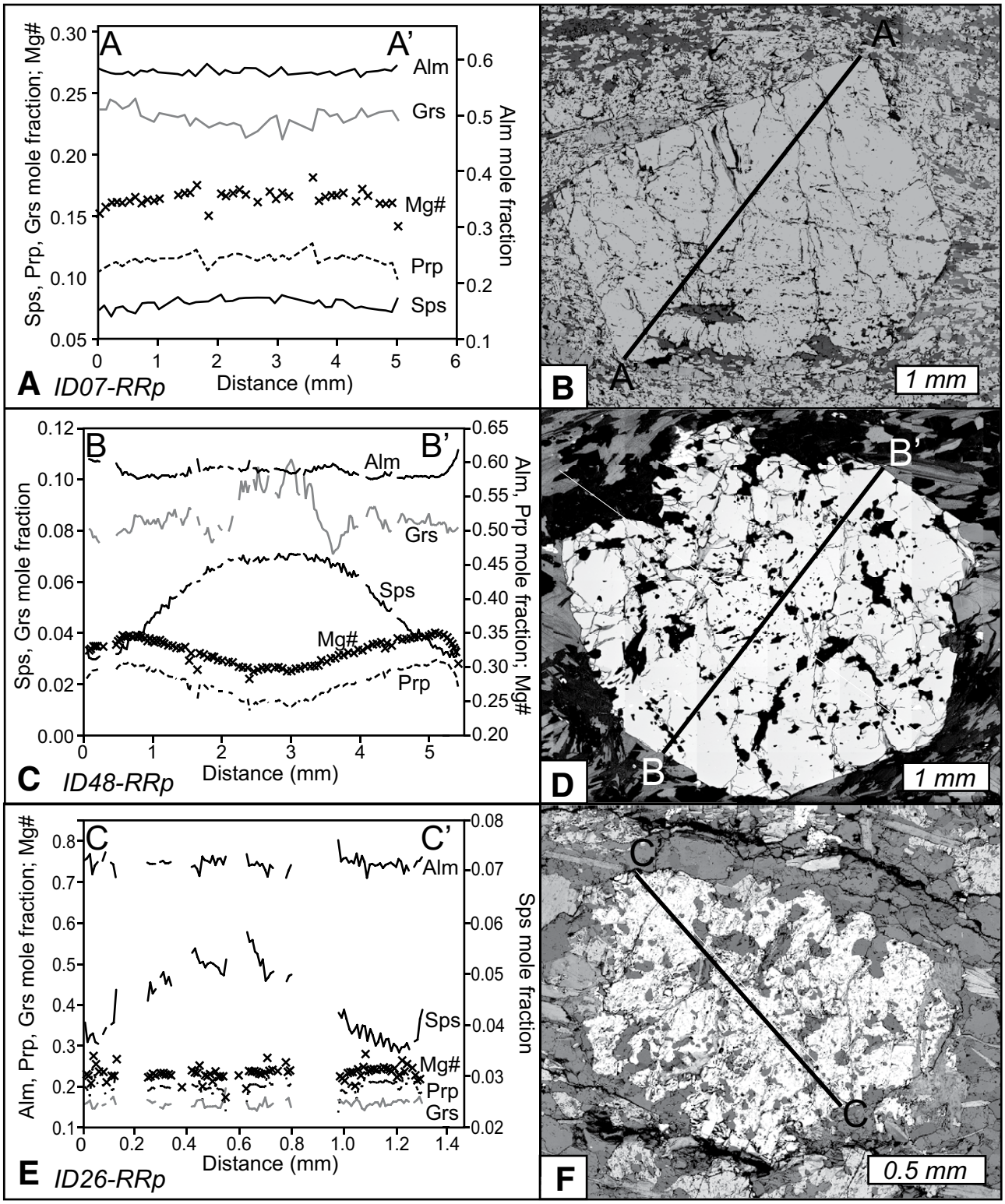

Figure 5. Rapid River garnet compositions from rim to rim along lines shown in backscatter electron (BSE) images. Garnet display weak compositional zoning. RRp—Rapid River plate; Alm—almandine; Grs—grossular; Prp—pyrope; Sps—spessartine. (A) ID07 line scan (n = 39). (B) ID07 (BSE). (C) ID48 line scan (n = 99). (D) ID48 (BSE). (E) ID26 line scan (n = 77). (F) ID26 (BSE).

preserved prograde growth zoning; however, the small decrease in Mg# could indicate diffusional resetting.

Petrography: ID48

The eastern limb of the Lake Creek antiform (Fig. 2) contains a heterogeneous sequence of interlayered biotite schist, calc-silicate gneiss, amphibole-bearing biotite gneiss, and amphibolite (Hamilton, 1969; Onasch, 1977; Bruce, 1998). Prior investigations in the Riggins region (Aliberti, 1988; Blake, 1991; Selverstone et al., 1992) placed these rocks in the hanging-wall block of the Pollock Mountain thrust fault, which projects ~30 km northeast from garnet locality ID03 into the Salmon River canyon (<0.25 km west of Ruby Rapids; Fig. 2). Lithologic heterogeneity in this area (Hamilton, 1969) may represent mixing of fault slices from the Rapid River and Pollock Mountain plates. In our study, chlorite-biotite–rich schists containing lesser amounts of amphibole are assigned to the Rapid River plate, and calc-silicate and amphibole-rich gneisses and amphibolites are assigned to the Pollock Mountain plate. Therefore, because it is a chlorite- and biotite-rich schist, ID48 is interpreted as part of the Rapid River plate.

Sample ID48 contains anhedral to subhedral garnet with hornblende, biotite, chlorite, kyanite, staurolite, rutile, plagioclase, and quartz that form a weakly developed schistosity that appears to be parallel to the trace of S_1. The garnet mode is ~12%. Garnet cores contain inclusions of staurolite, biotite, chlorite, rutile, plagioclase, and quartz; however, kyanite is only observed in garnet rims and in the matrix. Garnet porphyroblasts are partially wrapped by a biotite-chlorite–defined, synmetamorphic foliation suggesting garnet growth as an early metamorphic phase. Amphibole appears to be late, and replaces biotite and chlorite.

Garnet are zoned in almandine, spessartine, pyrope, and Mg# (Figs. 5C, 5D). Decreasing spessartine and increasing Mg# indicate that garnet zoning is the result of prograde growth and not strongly affected by diffusion. Grossular is slightly zoned with a low grossular core, increasing toward the rim, and then decreasing toward the matrix. Pyrope content increases toward the rim and almandine is unzoned. Increasing spessartine and almandine and decreasing pyrope are interpreted as resorption of garnet and diffusion along the garnet-matrix contact (Fig. 5C).

Petrography: ID26

Sample ID26 was collected from the Squaw Creek Schist ~2 km southwest of Riggins, Idaho (Fig. 1), and contains garnet, hornblende, biotite, titanite, ilmenite, plagioclase, and quartz. This sample was collected near the westernmost edge of garnet stability, based on isograds from Hamilton (1969). Medium-grained (2–5 mm) inclusion-rich anhedral garnet porphyroblasts show elongation parallel to the trace of foliation (S_1) defined by aligned biotite and hornblende. The garnet mode is ~4%. Inclusions in garnet have no preferred orientation and include titanite, hornblende, biotite, quartz, plagioclase, and ilmenite (Fig. 5F). Titanite is restricted to garnet inclusions and is absent in the peak matrix assemblage.

Garnet compositional zoning (Figs. 5E, 5F) shows decreases in spessartine from core to rim. However, almandine, pyrope, grossular, and Mg# are unzoned. Garnet from this sample contains the highest almandine content (~0.75 mol fraction almandine) analyzed in this study. Increases in spessartine at the rim that extend ~200 µm into the crystal (Fig. 5E) are interpreted as diffusion of Mn back into garnet during resorption.

P-T PATHS

Amphibolite and schist whole rock samples were analyzed using the Philips PW 2400 X-Ray fluorescence (XRF) spectrometer at the University of Alabama. Analytical methods follow those described by Stowell et al. (2010); rock compositions are given in Table DR2. Isochemical phase diagrams were constructed from whole-rock data in the Mn, Na, Ca, K, Fe, Mg, Al, Si, H, Ti, O chemical system using the Theriak-Domino software (de Capitani and Brown, 1987; de Capitani and Petrakakis, 2010) with thermodynamic data from the Holland and Powell (1998) database (dataset version 5.5) and solid solution activity models for garnet, biotite (White et al., 2007), plagioclase (Holland and Powell, 2004), chlorite (Powell and Holland, 1999; Tinkham et al., 2001), white mica (Coggon and Holland, 2002), ilmenite (White et al., 2005), clinoamphibole, orthoamphibole, clinopyroxene (Diener and Powell, 2007), orthopyroxene (White et al., 2002; Powell and Holland, 1999), epidote, cordierite, staurolite, and chloritoid (Holland and Powell, 1998). Oxygen was assigned using Theriak-Domino based mineral stoichiometry. Fe^{3+} was not considered based on the lack of Fe-rich epidote and magnetite in these rocks. The rocks were assumed to be water saturated based on the abundance of hydrous phases, commonly ≥50% amphibole and biotite. This assumption is further justified by water content versus temperature plots constructed in Theriak-Domino that suggest that observed mineral assemblages would be stable in a water-saturated system. *P-T* phase diagram models were constructed to predict equilibrium mineral assemblages and garnet composition isopleths. Garnet core compositions determined from electron microprobe analyses were plotted on each pseudosection to determine equilibration conditions for the start of garnet growth. To test the sensitivity of garnet fractionation on peak field assemblages and conditions in *P-T* models, ~80% of the observed garnet mode was fractionated out of the bulk composition for the highest garnet-mode sample (ID48). The resulting composition was remodeled to observe any change in the shape, size, or location of the peak field. Results showed very little variation between models (see Figs. DR1–DR2 for model results). Therefore, we assume that garnet fractionation does not affect peak assemblage temperature estimates in our models.

Pressures and temperatures were calculated using the AvePT module within the Thermo-Calc program (www.metamorph.geo.uni-mainz.de/thermocalc/) to constrain peak pressures for two samples (Powell and Holland, 1994), ID03 and ID07 (mineral compositions reported in Table DR3A). This provides additional *P-T* constraints on metamorphism that do not depend on the effective bulk composition of the rocks during mineral equilibration. The average composition of garnet rim and minerals interpreted to be in equilibrium with garnet rim were input into the program AX2 (Holland and Powell, 2000) to calculate end-member mineral activities at pressure and temperature. Rim analyses that may have been affected by diffusion were avoided. For AX2 calculations, pressure was specified at 8 kbar and temperature varied depending on the sample, based on conventional thermobarometry described in the following. For ID03 the garnet-biotite thermometer was used to constrain peak temperature, which averaged 650 °C. ID07 does not contain biotite and the peak temperature was instead assumed to be less than solidus conditions (<750 °C). AX2 activities were then input into the Thermo-Calc program AvePT module and were run at a range of temperatures based on peak assemblages from Theriak-Domino and thermometry. Results were overlain on the isochemical phase diagrams to further constrain peak conditions along the *P-T* paths for samples ID03 and ID07 (see Table DR3B for results and errors).

For samples with large peak assemblage fields, peak pressures and temperatures were further constrained using conventional thermobarometry, including garnet-aluminosilicate-plagioclase (GASP) for sample ID48 and garnet-biotite-hornblende-plagioclase for sample ID03 (Newton and Haselton, 1981; Koziol and Newton, 1988; Spear, 1993). The average composition of garnet rims (excluding diffused rims) and minerals that petrographically appear to be in equilibrium with garnet rims were used to calculate pressure and temperature. Activities were calculated for

almandine, pyrope, grossular (Hodges and Royden, 1984), annite, anorthite (Hodges and Spear, 1982), and amphibole (Kohn and Spear, 1989). Similarly to AvePT, results were overlain on the isochemical phase diagram to provide additional controls on *P-T* conditions (see Table DR3B).

Pollock Mountain Plate

The *P-T* path for ID23 from north of Pollock Mountain (Fig. 1) was determined from mineral inclusions in garnet, garnet core equilibration, and the peak assemblage (Fig. 6A). Inclusions in garnet of staurolite, biotite, chlorite, plagioclase, quartz, and rutile define the starting assemblage for garnet equilibration at 575–625 °C and 4.5–7 kbar (tan field, Fig. 6A). Garnet core compositional isopleths (0.56 almandine, 0.18 pyrope, 0.08 grossular, 0.18 spessartine) intersect at 550–600 °C and 5.3–5.8 kbar, which overlaps with the assemblage inferred from inclusions in garnet (yellow ellipse, Fig. 6A). The peak assemblage (garnet, biotite, kyanite, plagioclase, and quartz) is stable at 625–675 °C and 6.5–9.3 kbar (pink field, Fig. 6A). Garnet core equilibration is above the garnet-in reaction, which is not predicted within the *P-T* space, extends down to 500 °C (Fig. 6A). The resulting *P-T* path extends from 550 to 600 °C and 5.3–5.8 kbar to 625–675 °C and 6.5–9.3 kbar (Fig. 6A).

The *P-T* path for sample ID03, from Cold Springs Saddle just south of Pollock Mountain (Figs. 1 and 2), is constrained by mineral inclusions in garnet and the peak assemblage, garnet core isopleth intersection, and thermobarometry results. The initial growth of garnet is constrained to fall in a mineral assemblage inferred from inclusions and contains garnet, clinoamphibole, biotite, plagioclase, and ilmenite (tan field in Fig. 6B). Garnet core isopleths (0.60 almandine, 0.20 pyrope, 0.11 grossular, and 0.08 spessartine) intersect within the aforementioned inclusion assemblage. This result indicates that garnet core equilibrated at 650–750 °C and 5.5–7 kbar. The peak assemblage, garnet, clinoamphibole, biotite, plagioclase, quartz, and rutile, is shown as the pink field in Figure 6B. This assemblage field occupies a large *P-T* space, 600–750 °C and 7.5–11 kbar. AvePT and thermobarometry calculations for minerals in equilibrium with nondiffused garnet rims overlap and indicate *P-T* estimates of 650–720 °C and 7.2–7.7 kbar that overlap with the peak field at conditions of 650–700 °C and ~7.5 kbar. Garnet core inclusions and composition *P-T* estimates greatly overstep the garnet-in reaction, making the earliest *P-T* history of this sample ambiguous. *P-T* estimates indicate a near-isothermal, increasing-pressure *P-T* path from 650 to 750 °C and 5.5–7 kbar to 650–700 °C and 7.5–8.5 kbar, suggesting an increase in pressure of ~1.5 kbar (Fig. 6B).

Rapid River Plate

The *P-T* path for sample ID07 is constrained from mineral inclusions in garnet, garnet core composition, peak assemblage, and thermobarometry. The tan field in Figure 6C indicates the assemblage inferred from inclusions of clinoamphibole, plagioclase, quartz, and ilmenite within garnet. This field is the earliest identifiable assemblage and overlaps with garnet core compositional isopleths (0.57 almandine, 0.12 pyrope, 0.23 grossular, 0.08 spessartine) at 625–650 °C and 6.3–6.8 kbar. The peak assemblage (garnet, clinoamphibole, zoisite, plagioclase, quartz, rutile) equilibrated between 525 and 650 °C and 7.5 and 11 kbar. Thermobarometry estimates conducted on phases in equilibrium with garnet rim indicate conditions of 600–700 °C and 7.6–8.8 kbar that overlap with the peak assemblage at 600 °C and ~8.8 kbar. Garnet core equilibration conditions are significantly above the predicted garnet-in reaction. The *P-T* path for ID07 is 625–650 °C and 6.3–6.8 kbar to 600 °C and ~8.8 kbar, indicating a pressure increase of ~2 kbar.

P-T conditions for sample ID48 were determined from inclusions in garnet, garnet core composition, and peak assemblage. Inclusions in garnet are staurolite, biotite, chlorite, plagioclase, quartz, and rutile, which for this bulk composition is constrained at 575–650 °C and 5–8.3 kbar. This assemblage defines the first assemblage with which garnet was in equilibrium (tan field, Fig. 6D). The peak assemblage is garnet, clinoamphibole, biotite, kyanite, plagioclase, quartz, and rutile (pink field, Fig. 6D), 660–710 °C and 7.3–11 kbar. Garnet core compositional isopleths (0.59 almandine, 0.25 pyrope, 0.09 grossular, 0.07 spessartine) are subparallel with respect to temperature and define a broad area for garnet core equilibration that overlaps with the garnet inclusion assemblage (yellow ellipse, Fig. 6D) at 590–640 °C and 6.0–8.7 kbar. Similar to other samples, the garnet core isopleths are overstepped by ~200 °C. Due to overlap with both assemblages, the garnet core isopleths do not help constrain precise *P-T* conditions for the start of garnet growth; however, they indicate a lower temperature than the peak assemblage. Thermobarometry (GASP) calculations indicate conditions of 724 °C and 10.4 kbar, plotted with errors of 50 °C and 1 kbar. These estimates overlap with peak assemblages between 675 and 700 °C and 9.5 and 10 kbar. Therefore, the *P-T* path for this sample is from 580–640 °C and 6.0–8.3 kbar to 660–700 °C and 9.5–10 kbar, a change of ~70 °C and 3 kbar.

The sample ID26 *P-T* path was constrained using titanite and ilmenite stability, garnet core isopleths, and the peak assemblage. Titanite, present only as inclusions in garnet, and ilmenite define the earliest stability region for garnet equilibration and are both stable together in a narrow field between 510 and 530 °C and 5 and 7 kbar (tan field, Fig. 6E). Therefore, the earliest part of the *P-T* path is likely ~6 kbar and 520 °C. Other inclusions in garnet are clinoamphibole, biotite, plagioclase, quartz, and ilmenite; these are the same minerals present in the matrix and define the peak assemblage (pink field, Fig. 6E), stable at 575–700 °C and 7–9.5 kbar. Garnet core isopleths (0.68 almandine, 0.15 pyrope, 0.14 grossular, 0.06 spessartine) for this sample do not overlap with the proposed initial garnet equilibration assemblage and instead overlap with the peak assemblage at 600–675 °C and 7–8.5 kbar. Lack of garnet core isopleth intersection with the initial assemblage could be due to garnet-in overstepping issues, as reported for other samples in this study, or could be due to problems with the thermodynamic data used to construct isochemical phase diagrams. The *P-T* path for sample ID26 transits from ~520 °C and 6 kbar to 600–675 °C and 7–8.5 kbar, a change of ~200 °C and 2 kbar.

Sm-Nd AND U-PB GEOCHRONOLOGY

Garnet Sm-Nd Geochronology Methods

Sm and Nd isotope ratios (Table DR4) for garnet (bulk and single crystal), matrix (whole rock minus garnet), and whole-rock aliquots were used to construct isochrons that are interpreted to represent the age of garnet growth. Sample preparation, Sm and Nd concentrations, and mass spectrometry generally followed the methods described in Stowell and Tinkham (2003). Crushed garnet separates were run through a Franz isodynamic magnetic separator at ~0.65 A with a 10° side angle to remove non-garnet. The resulting garnet fractions were hand-picked to remove visible impurities and sieved. Sieved garnet fragments were partly dissolved in hydrofluoric and perchloric acid in order to remove silicate and phosphate inclusions, respectively. These partial dissolution steps (Table DR5) are similar to those described in Pollington and Baxter (2011). Isotope ratios were obtained on a VG Sector 54 thermal ionization mass spectrometer (TIMS) at the University of North Carolina at Chapel Hill with the exception of sample ID26, which was obtained on a VG Sector 54 TIMS at the University of Alabama RadioIsotope Lab. Four ages

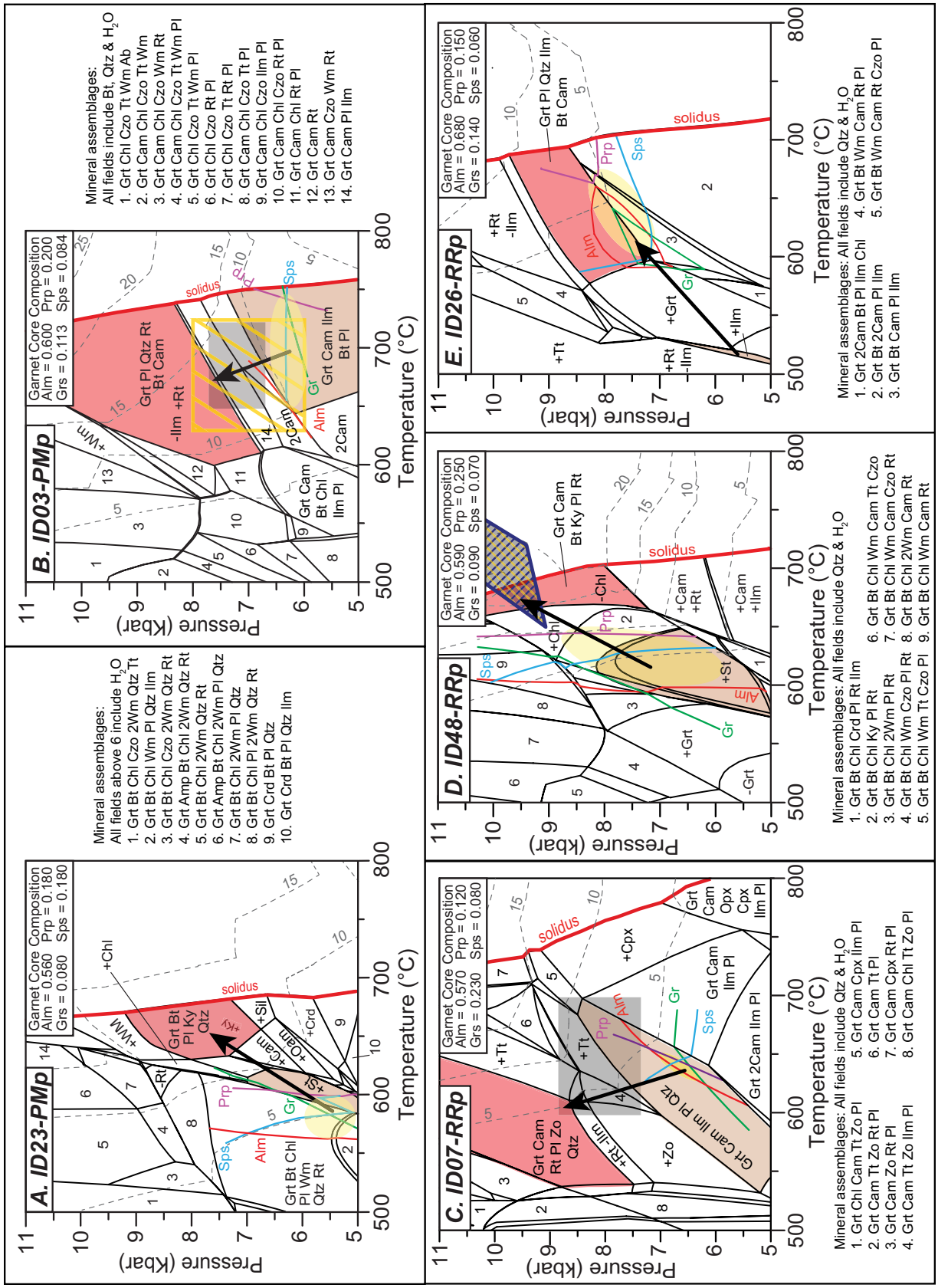

Figure 6. Pressure-temperature (*P-T*) isochemical phase diagrams for garnet amphibolites and schists from the Salmon River suture zone in western Idaho. *P-T* paths were determined from initial garnet growth conditions from the intersection of garnet compositional isopleths calculated for observed core compositions and peak metamorphic conditions estimated from mineral rim thermobarometry. Pink fields—peak assemblages; tan fields—earliest observable assemblage from inclusions in garnet. Yellow ellipse indicates best intersection for garnet core compositional isopleths. Boxes indicates results from AvePT (gray; Thermo-Calc program, www.metamorph.geo.uni-mainz.de/thermocalc/), GASP (garnet-aluminosilicate-plagioclase; blue hachure area), and GBHP (garnet-biotite-hornblende-plagioclase; yellow hachure area) thermobarometry. See text for details. (A) ID23, Pollock Mountain plate (PMp). (B) ID03, PMp. (C) ID07, Rapid River plate (RRp). (D) ID48, RRp. (E) ID26, RRp. Abbreviations after Kretz (1983): Bt—biotite; Cam—clinoamphibole; Chl—chlorite; Cpx—clinopyroxene; Crd—cordierite; Czo—clinozoisite; Grt—garnet; Ilm—ilmenite; Ky—kyanite; Pl—plagioclase; Qtz—quartz; Rt—rutile; Tt—titanite; Wm—white mica; Zo—zoisite.

and one low-precision, yet corroborating, isochron were determined for amphibolite and schist from the Salmon River suture zone.

Sm-Nd Garnet Ages from the Pollock Mountain Plate

Garnets from sample ID23 were microsampled using a Dremel hand drill and cutting tool to mechanically separate garnet geometric and geochemical cores from rim material so that the duration of garnet growth could be assessed. Ages were initially calculated with garnet core-rock and rim-rock combinations. However, isotopic ratios for cores of three garnet grains are dissimilar, and the garnet B core is more similar to rim values from other grains. Therefore, we infer that some garnet core samples do not include the oldest center of grains and/or that some grains grew later. Isotope ratios for garnet C core, rock matrix, and whole rock are on a 3-point isochron of 135 ± 2.4 Ma. Isotope ratios for the rock matrix, whole rock, garnet B core, and garnet C rim produce a 4-point isochron age (Fig. 7A) of 123.9 ± 1.3 Ma.

Sm and Nd isotope data for two-stage garnet from sample ID03 from the Pollock Mountain plate were collected for three garnet and whole rock and matrix splits. Garnet 3 is a single crystal garnet core that was

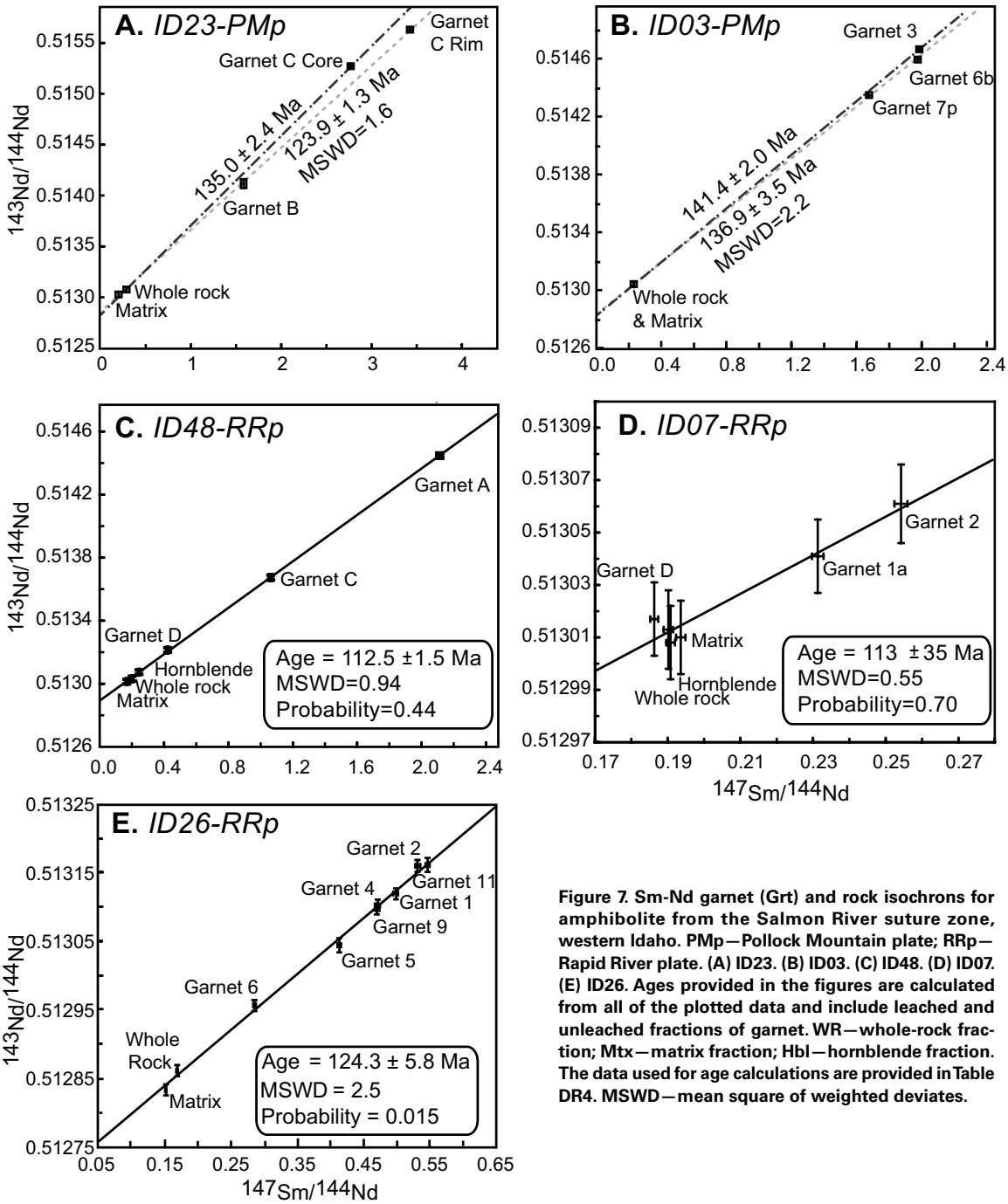

Figure 7. Sm-Nd garnet (Grt) and rock isochrons for amphibolite from the Salmon River suture zone, western Idaho. PMp—Pollock Mountain plate; RRp—Rapid River plate. (A) ID23. (B) ID03. (C) ID48. (D) ID07. (E) ID26. Ages provided in the figures are calculated from all of the plotted data and include leached and unleached fractions of garnet. WR—whole-rock fraction; Mtx—matrix fraction; Hbl—hornblende fraction. The data used for age calculations are provided in Table DR4. MSWD—mean square of weighted deviates.

extracted using a computer-guided micromill to separate the chemically and texturally defined core from the rim. Isotope ratios for the garnet 3 core combined with the whole rock and matrix produced an age of 141.4 ± 2.0 Ma (Fig. 7B). This result is effectively based on 2 points because the matrix and whole-rock samples are indistinguishable. Garnet grains 6b and 7p were extracted using a Dremel hand grinder in order to spatially remove rim material and obtain inclusion-free garnet core material. These garnet core separates (garnet grains 6b and 7p) define a 3-point isochron with an age of 136.9 ± 3.5 Ma. The span of ages for sample ID23 (135–124 Ma) and sample ID03 (141–137 Ma) indicate a best estimate for garnet growth in this part of the Pollock Mountain plate as 141–124 Ma.

Sm-Nd Garnet Ages from the Rapid River Plate

Sample ID48 and ID07 garnet Sm-Nd ages for the Rapid River plate are considered together here due to age similarities. Sample ID48 produced a 6-point isochron (whole rock, matrix, hornblende, and three whole garnet separates: garnet D, garnet C, garnet A) with an age of 112.5 ± 1.5 Ma (Fig. 7C). A second sample, ID07, produced a poor precision isochron (Fig. 7D) resulting from very low garnet $^{147}Sm/^{144}Nd$ ratios (<0.26) and a small spread (0.18–0.26) between these ratios and those of the whole rocks. Although the precision of individual analyses is high, the range between garnet and whole rock isotopic ratios is very small, resulting in high uncertainty. The high uncertainty is likely due to inclusions in garnet that were not removed during the partial dissolution process, resulting in garnet separates yielding low $^{147}Sm/^{144}Nd$ for ID07. Apatite and clinozoisite inclusions are the only minerals identified in the garnet that are likely to incorporate a significant mass of REEs. Presumably, tiny grains throughout the garnet were not removed during the partial dissolution. Although the uncertainty is very large, the age of 113 ± 35 Ma overlaps with the high-precision age determined for ID48 (112.5 ± 1.5 Ma) and a Lu-Hf age of 111 ± 11 Ma from a similar locality within the Berg Creek Amphibolite reported by Wilford (2012).

Sample ID26 produced a 9-point isochron (whole rock, matrix, and 7 bulk garnet separates) with an age of 124.3 ± 5.8 Ma (Fig. 7E). Because of the large variety and volume of inclusions, multiple garnet grains were sampled in bulk and each separate was leached differently (detailed in Table DR5). The uncertainty of ± 5.8 Ma is due to low $^{147}Sm/^{144}Nd$ ratios (<0.60) rather than low precision of the Nd isotope ratios. This is probably a result of incomplete inclusion removal despite the partial dissolution steps.

U-Pb Zircon Geochronology

U-Pb zircon ages for four pluton samples (PRC01, ID04, ID42, and ID58) provide a comparison with garnet ages and a means to evaluate possible plutonic contributions to heating during metamorphism, timing of deformation, and age of metamorphism. U-Pb zircon isotope ratios were obtained for PRC01, ID04, and ID42 using the Nu Plasma laser ablation–multicollector–inductively coupled plasma–mass spectrometer (LA-MC-ICP-MS) in the University of Arizona LaserChron laboratory using techniques described by Gehrels et al. (2008), with beam diameters ranging between 12 and 30 µm. Isotope ratios and ages for each spot analysis are provided in Tables DR6–DR9. Error-weighted averages of $^{206}Pb/^{238}U$ ages were calculated and plotted using Isoplot (Ludwig, 2003) and then systematic errors were incorporated into the average age uncertainties (Figs. 8A–8D) with uncertainties presented at 95% confidence levels. U-Pb zircon isotope ratios were obtained for ID58 on a Thermo Scientific ELEMENT2 equipped with a 193 Ar-F excimer laser at the California State University Northridge (following methods in Chang et al., 2006). Analyses were conducted during a single analytical session with a beam diameter of ~30–40 µm. Individual spot analyses (reported in Tables DR6–DR9) include propagated analytical and systematic errors. Dates were corrected for minor amounts of common Pb (following methods in Compston et al., 1984). Weighted average age plots were constructed in Isoplot (Ludwig, 2003).

Sample ID42 is from a medium-grained biotite-hornblende orthogneiss in the Pollock Mountain plate collected ~240 m east of ID03. Zircons are prismatic and cathodoluminescence (CL) images show relatively simple oscillatory zoning with narrow apparently unzoned rims (15–40 µm). Because U/Th can be used to distinguish metamorphic (high U/Th) and igneous (low U/Th) zircon grains (Vavra et al., 1999), age populations were defined based on U/Th in zircon. Analyses of low U/Th zircon cores define an age (Fig. 8A) of 206.3 ± 3.0 Ma (n = 79). Analyses of high U/Th rims (23 to ~6000) yield dates ranging from 207 to 133 Ma. The error-weighted average age of 9 high U/Th rim analyses (Fig. 8A) is 140.5 ± 3.9 Ma, which is indistinguishable from garnet core Sm-Nd ages (141–137 Ma) discussed herein.

Sample ID58 is a medium-grained tonalite that crops out ~11.25 km north-northeast of Pollock Mountain (Fig. 1) and is structurally part of the Pollock Mountain plate (Lund, 2004). This deformed tonalite is truncated to the north and west by the Pollock Mountain thrust fault (Lund, 2004) and was collected to constrain the timing of juxtaposition of the Pollock Mountain and Rapid River plates. Zircons from ID58 are prismatic and have well-developed oscillatory zoning in CL images. We analyzed 27 zircons, the majority of which are concordant or slightly discordant (see Table DR9). The error-weighted average age of 24 zircons is 117.1 ± 1.8 Ma (Fig. 8B). Three older outliers are interpreted as xenocrystic (ages of 128.6, 129.2, and 132.6 Ma).

Samples PRC01 and ID04 were dated in order to evaluate possible heating from plutons along the eastern edge of the Salmon River suture zone. An undeformed biotite-hornblende tonalite from the Payette River complex (PRC01; Fig. 8C) contained oscillatory zoned zircon that yielded a weighted mean age of 90.4 ± 0.8 Ma (n = 25). A moderately deformed orthogneiss from the Little Goose Creek Complex (ID04; Fig. 8D) was collected just east of the Pollock Mountain plate along the Salmon River. ID04 is dominated by high U/Th zircon (U/Th > 10) dated between 111 and 100 Ma that yield a weighted mean age of 108.1 ± 1.8 Ma (n = 16); 3 ca. 135 Ma grains that displayed high U/Th were interpreted as xenocrysts and thus excluded from the weighted mean calculation.

DISCUSSION

Timing of Western Idaho Tectonism

The earliest ages for metamorphism in the Salmon River suture zone are derived from the Pollock Mountain plate. Our data indicate that metamorphism began ca. 141 Ma and persisted until at least 124 Ma. The upper limit for garnet core growth at 141.4 ± 2.0 Ma and younger core isochron ages of 137 Ma from ID03 are consistent with the 144 Ma age (uncertainties unspecified) reported in Getty et al. (1993). The 141–137 Ma garnet ages for metamorphism are also corroborated by our new $^{206}Pb/^{238}U$ zircon rim ages (140.5 ± 5.1 Ma from sample ID42), which are inferred to be metamorphic based on U/Th ratios >5 (Fig. 9; e.g., Vavra et al., 1999). Therefore, the new age range of 141–137 Ma reported here for garnet core growth provides a robust estimate for the timing of initial garnet growth in the Pollock Mountain plate. Our Sm-Nd garnet core and rim ages from sample ID23 (i.e., ca. 135 and ca. 124 Ma, respectively) suggest that some garnet in the Pollock Mountain plate may have grown over a period of 10 m.y. or longer. If garnet grains within this age range

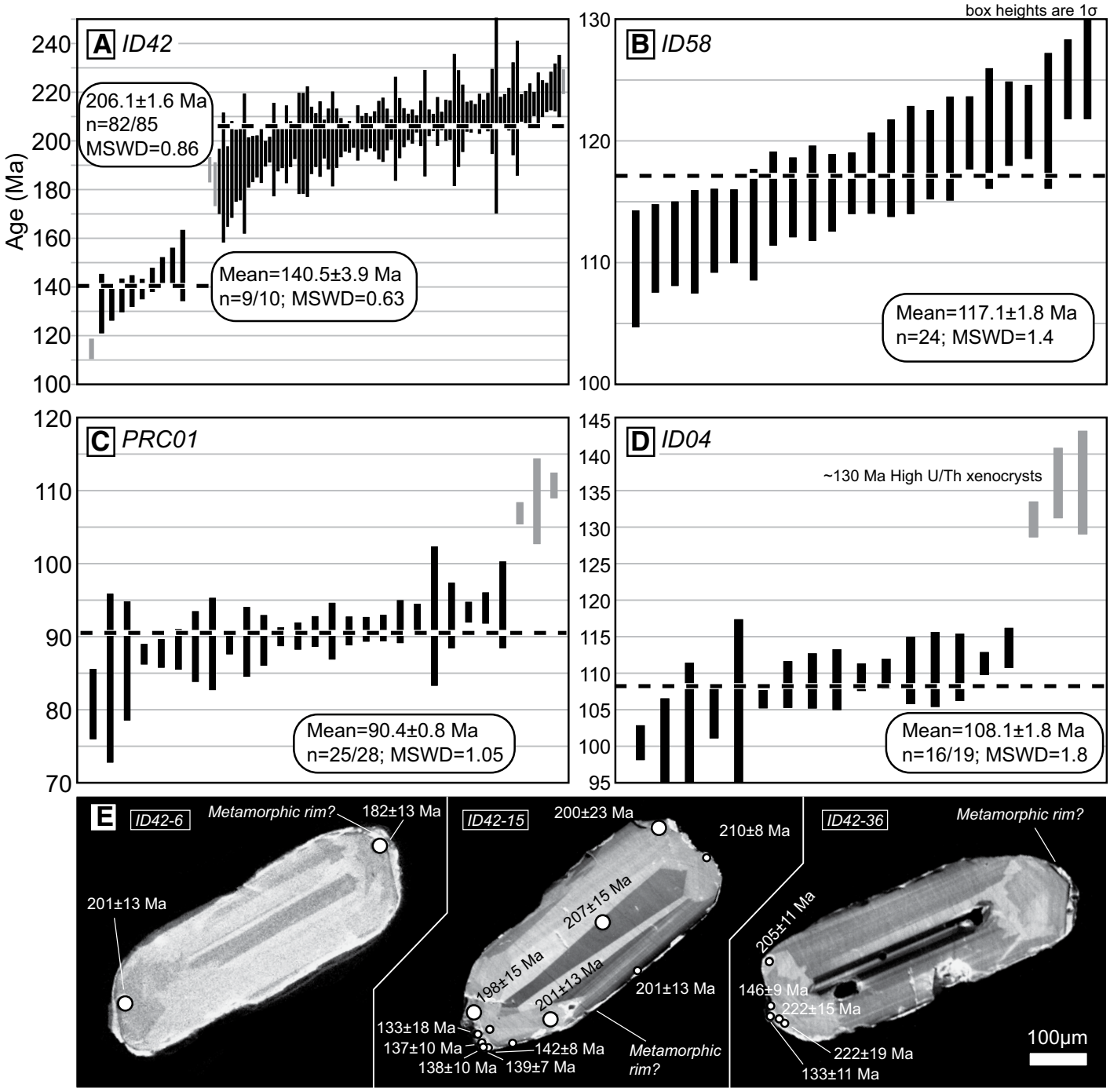

Figure 8. Error-weighted average $^{206}Pb/^{238}U$ ages of zircon populations. (A) ID42. (B) ID58. (C) PRC01. (D) ID04. (E) Cathodoluminescence images of zircon grains from ID42 with approximate laser analytical spots and ages. MSWD—mean square of weighted deviates.

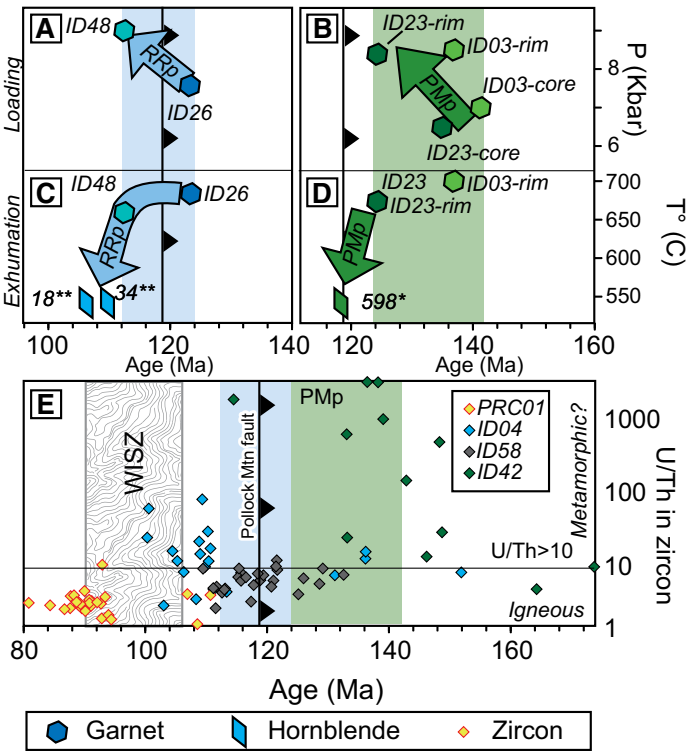

Figure 9. Interpretive summary of geochronology, thermochronology, and pressure-temperature (*P-T*) data. (A) Prograde loading of the Rapid River plate (RRp) from ~7–9 kbar during 123–113 Ma metamorphism. (B) Prograde loading of the Pollock Mountain plate (PMp) from ~6.5 kbar to ~8.5 kbar during 141–124 Ma metamorphism. (C) RRp cooling from ~650 °C at 113 Ma to <550 °C by 109 Ma. (D) PMp cools from ~675 °C at 124 Ma to <550 °C at 118 Ma. (E) High U/Th (>10) zircon analyses may indicate metamorphism spanned the gap from 141 to 113 Ma Salmon River suture metamorphism into western Idaho shear zone (WISZ) deformation (105–91 Ma; Giorgis et al., 2008).

had not been microsampled, the result might have been a mixed age similar to the previously reported 128 Ma garnet age (Getty et al., 1993). The oldest garnet from ID23 (ca. 135 Ma) is within error of the youngest age estimates (ca. 136.9 Ma) for two-stage garnet cores from ID03, both within the Pollock Mountain plate. Due to the large aliquot of garnet (>20 mg; Table DR5) used for the Sm-Nd geochronology reported here, ages are likely derived from garnet with a significant age range. Therefore, apparent ages may represent averages of different proportions of age-zoned garnet. In this context, different Sm-Nd ages may be interpreted as distinct metamorphic events (i.e., terrane amalgamation followed by accretion or docking with Laurentia; Getty et al., 1993). In contrast, we propose that garnet growth in the Pollock Mountain plate could have resulted from one long-lived tectonothermal event beginning between 141 and 137 Ma and continuing until ca. 124 Ma, based on our overlapping Sm-Nd garnet ages from two localities (ID03, ID23) and the corroborating U/Th $^{206}Pb/^{238}U$ zircon age (ca. 140 Ma) (Fig. 9). Hornblende $^{40}Ar/^{39}Ar$ data record cooling below 525 °C ca. 119–118 Ma, requiring the conclusion of prograde metamorphism in the Pollock Mountain plate to have occurred by that time (Lund and Snee, 1988; Getty et al., 1993). The weakly to unmetamorphosed tonalite (ID58; Fig. 1) cut by the Pollock Mountain thrust fault also suggests that metamorphism in the Pollock Mountain plate had locally ceased by 117 Ma. Exhumation and additional cooling may have coincided with movement along the Pollock Mountain thrust fault after 117 Ma, bracketing the duration of Pollock Mountain metamorphism from 141 to 118 Ma. Given that synmetamorphic foliation in the Pollock Mountain amphibolite and Hazard Creek Complex ($^{206}Pb/^{238}U$ zircon = 118 ± 5 Ma; Manduca et al., 1993) are continuous across the lithologic contact (Pollock Mountain amphibolite–Hazard Creek Complex plate; Fig. 2B), ductile deformation in this area was active through ca. 118 Ma, deforming both units during post-peak metamorphic cooling in the Pollock Mountain plate.

Garnet from the Rapid River plate records metamorphism that began during the waning stages of Pollock Mountain metamorphism ca. 124 Ma (ID26) and continued until at least ca. 113 Ma (ID48), >10 m.y. after the youngest recorded metamorphism in the Pollock Mountain plate. These dates expand the documented duration of garnet zone and higher grade metamorphism in the Salmon River suture zone from 13 m.y. (144–128 Ma; Getty et al., 1993) to ~31 m.y. (144–113 Ma; Getty et al., 1993; this study). Our 117 Ma age for syndeformational pluton emplacement along the Pollock Mountain thrust fault (ID58) and ca. 119–118 Ma hornblende cooling ages for the overriding Pollock Mountain plate (Lund and Snee, 1988; Snee et al., 1995; Getty et al., 1993) are synchronous with ca. 124–113 Ma garnet growth in the Rapid River plate. This suggests that juxtaposition of the two plates occurred during postmetamorphic cooling in much or all of the Pollock Mountain plate ca. 119–117 Ma, but during prograde metamorphism of the Rapid River plate. Metamorphism in the Rapid River plate ceased following 113 Ma garnet growth and prior to ca. 109–107 Ma cooling of syntectonic hornblende below ~525 °C (Lund and Snee, 1988), constraining the duration of metamorphism in the Rapid River plate to ~15 m.y. (i.e., from early garnet growth to postmetamorphic cooling of hornblende).

Salmon River Suture Zone Metamorphism

P-T paths suggest that both the Pollock Mountain and Rapid River plates record Cretaceous isothermal loading of >2 kbar at 600–700 °C. These estimates are compatible with previously published estimates for metamorphic conditions in the Pollock Mountain and Rapid River plates by Selverstone et al. (1992) and Getty et al. (1993); their results, however, indicated loading within the Pollock Mountain plate to as much as 11 kbar, with little evidence for loading in the adjacent Rapid River plate, as the new data suggest. Geochronology and *P-T* estimates (141–124 Ma and ~5 kbar for the Pollock Mountain plate; 124–113 Ma and ~3 kbar in the Rapid River plate), suggest loading rates of ~1 mm/yr. We interpret that isothermal loading within the Salmon River suture zone was controlled by thrust stacking that drove metamorphism in structural sheets (Rapid River and Heavens Gate plates) underlying the Pollock Mountain plate in a fashion similar to that described in the northern (Spear et al., 1990) and central Appalachians (Bosbyshell et al., 2016). In the central Appalachians, metamorphism was synchronous with nappe emplacement, fault displacement, and loading (e.g., van Staal et al., 2008). In the Salmon River suture zone, crustal thickening via thrust loading was diachronous, with westward fault propagation occurring throughout the duration of Jurassic–Cretaceous tectonism along the western Laurentian margin.

In the thrust-loading model for metamorphism of the Salmon River suture zone (Fig. 10), magmatic heating is not required to drive metamorphism. The contribution of magmatic heat during metamorphism was likely negligible and is supported by the paucity of 140–119 Ma magmatism in the Salmon River suture zone, minor 128 Ma plutonism in the Wallowa terrane (Jeffcoat et al., 2013), and the minor presence of ca. 115–111 Ma plutonism near Riggins (Unruh et al., 2008), suggesting that there was little thermal contribution from plutonism during peak metamorphism. The Permian Chair Point pluton (Kauffman et al., 2011) predates Mesozoic metamorphism and the Hazard Creek Complex (ca. 118 Ma;

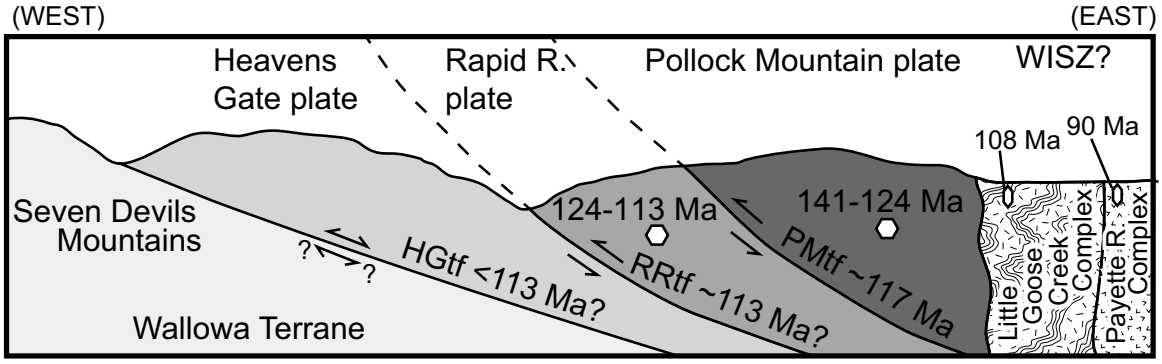

Figure 10. Generalized schematic cross section showing the temporal evolution of the Salmon River suture zone and western Idaho shear zone (WISZ). R.—river; HG—Heavens Gate; RR—Rapid River; PM—Pollock Mountain; tf—thrust fault.

Manduca, 1988) was emplaced during cooling of the Pollock Mountain plate and possibly during early Rapid River plate metamorphism. In addition, the Early Cretaceous Little Goose Creek Complex and Payette River complex exposed east of the Salmon River thrust sheets were emplaced ca. 111–105 Ma and ca. 90 Ma, respectively (Manduca et al., 1993; ID04, PRC01, this study; 99MG, Giorgis et al., 2008), which postdates peak metamorphism in the Salmon River suture zone. Small plutonic stocks that are coeval with late metamorphism in the Pollock Mountain plate (123 Ma and 118 Ma; Jeffcoat et al., 2013) are of limited areal extent and are exposed west of the Salmon River suture zone. *P-T* paths (Fig. 6) also suggest minor to no heating during prograde garnet zone metamorphism. Therefore, there are no known plutons of appropriate age or adequate size at the current level of exposure proximal to either of the two thrust sheets to provide sufficient heat to regionally metamorphose the Rapid River and Pollock Mountain plates to peak conditions.

The range of temperatures for initial garnet growth throughout the Salmon River suture zone indicated by loose garnet core isopleth (ID03, ID23, ID07, ID48, ID26) intersections are significantly higher (~50–200 °C) than the initial garnet-producing reaction (i.e., garnet-in line) predicted by isochemical phase diagrams (Fig. 6). This discrepancy between the model predicted garnet-in reaction and garnet isopleth core intersections may be due to postmetamorphic diffusion of garnet core compositions. This could be a result of a long-lived, high-heat thermal event that caused a long duration of garnet growth; this is supported based on the presence of garnet samples with a growth duration of ~10 m.y. However, some zoning features are preserved, including thin (<0.5 mm) diffusion features at the rim-matrix boundary in garnet from samples ID03, ID07, ID26, ID48. In addition, most samples show bell-shaped spessartine zoning that is usually indicative of preservation of the initial composition of the core. Kinetic overstepping, where initial garnet growth begins after garnet becomes a stable phase along the prograde *P-T* path, might also have caused the observed discrepancy in initial garnet growth estimates. Similar to early diffusion, this interpretation would also require high heat input. Previous studies (Gray and Oldow, 2005; McKay, 2011) postulated that volcanogenic protoliths in the Riggins region (e.g., Squaw Creek Schist) may represent part of a collapsed backarc. Deformation in collisional orogens is frequently focused in collapsing backarc regions, because these hot, weak areas are more ductile (Hyndman et al., 2005). High heat flow in a collapsing backarc setting (Stern, 2002; Watanabe et al., 2013) provides a plausible explanation for early heating. Therefore, prior to metamorphism, increased heat flow and an elevated geothermal gradient might be expected during early metamorphism of the Salmon River suture zone.

P-T paths from most samples show counterclockwise near-isothermal loading of ~2–3 kbar with little to no heating observed that might be expected with thermal relaxation following tectonic loading (Fig. 6). The lack of heating following thrusting would require either rapid exhumation or perturbation of the regional isotherms through thrust faulting that could be achieved through continued faulting. Rapid postmetamorphic cooling may also account for the interpretation of Selverstone et al. (1992) of garnet growth during exhumation and cooling in the Pollock Mountain plate. The presence of magmatic epidote in the 118–114 Ma Hazard Creek Complex that intrudes the Pollock Mountain plate, however, suggests that the Pollock Mountain plate was at depths of >8 kbar (Zen and Hammarstrom, 1984) during post-peak metamorphic cooling, which is not compatible with rapid exhumation. Unlike Selverstone et al. (1992), we propose that a thrust model for metamorphism does not require lithospheric delamination to account for the observed rapid postmetamorphic cooling in the Salmon River suture zone, because rapid cooling could be driven by thrust exhumation combined with erosion. If the Salmon River suture zone was subjected to high heat flow in a backarc setting prior to metamorphism, thermal relaxation following thrusting may have been offset by a relative decrease in heat flow with the transition from backarc extension to collisional orogenesis.

Tectonic Model for Cretaceous Metamorphism

Juxtaposition at or after 117 Ma of the older, higher grade Pollock Mountain plate rocks with the younger, lower grade metamorphic rocks of the Rapid River plate coincides with both prograde metamorphism in the footwall rocks of the Rapid River plate and exhumation in the hanging wall. Therefore, we postulate that late-stage metamorphism in the Salmon River suture zone was controlled by thrust faulting and crustal thickening. This model also explains the near-isothermal loading in the Rapid River plate and the juxtaposition of higher grade, older metamorphic rocks in the overlying Pollock Mountain plate. Similar processes may have driven metamorphism in the Pollock Mountain and Heavens Gate plates; however, any evidence for a thrust sheet overlying the Pollock Mountain plate has been removed by uplift along the arc-continent boundary, erosion, and/or intrusion of the Idaho batholith. Along the western side of the Salmon River suture zone, there are limited thermochronometry data; however, future work might resolve the age of metamorphism in low-grade metamorphic rocks in the Heavens Gate plate.

The new Sm-Nd garnet and U-Pb zircon ages presented here extend the duration of metamorphism in the Salmon River suture zone, with metamorphism persisting for at least 25–30 m.y. Following the cessation of

141–113 Ma (Early Cretaceous) metamorphism, compressional deformation persisted along the western Laurentian margin, as evidenced by mid-Cretaceous approximately east-west contractional structures assigned to the western Idaho shear zone (e.g., Giorgis et al., 2008). High U/Th ratios (>10) from zircon in ID04 (Figs. 8 and 9) suggest the presence of metamorphic fluids during syndeformational emplacement of the Little Goose Creek Complex; this suggests that metamorphism continued along the arc-continent boundary through 108 Ma. If peak metamorphism occurred throughout the western Idaho shear zone ca. 98 Ma (Braudy et al., 2017), then 108 Ma metamorphism in the Little Goose Creek Complex may represent the earliest phases of western Idaho shear zone metamorphism.

Although early deformation associated with offshore terrane accretion occurred ca. 159 Ma (Schwartz et al., 2011) in the Wallowa terrane, penetrative deformation continued into the mid-Cretaceous (e.g., Lund and Snee, 1988; Manduca et al., 1993) and involved oroclinal rotation at 140–126 Ma (Zák et al., 2015) coeval with metamorphism in the Pollock Mountain plate (141–124 Ma). Displacement (ca. 117 Ma or younger) on the Pollock Mountain fault, rotation and flattening of Pollock Mountain plate garnet, and metamorphism in the underlying Rapid River plate (ca. 113 Ma) record continued deformation in the Salmon River suture zone. The transition from 113 Ma metamorphism in the Salmon River suture zone to possible ca. 108 Ma metamorphism in the western Idaho shear zone suggests that metamorphism in the Salmon River suture zone and western Idaho shear zone either partially overlaps temporally or was separated by a very brief (<5 m.y.) interlude. In either case, contractional deformation and metamorphism in western Idaho likely occurred from before 141 Ma to after 108 Ma, and was characterized by thrust faulting in the Salmon River suture zone that possibly evolved into ductile extrusion along the arc-continent boundary. On this basis, we suggest that terrane accretion in western Idaho was a prolonged process (>30 m.y.), with metamorphism directly recording local structural development (i.e., thrust faulting) instead of individual terrane collisions.

CONCLUSIONS

Sm-Nd geochronologic results from microsampled garnet domains suggest a prolonged duration of metamorphism within the Pollock Mountain plate of the Salmon River suture zone, spanning 141 to 124 Ma, that was previously interpreted to represent two temporally distinct events, i.e., the offshore assembly of the Blue Mountains province and its subsequent docking with Laurentia. Based on new age and *P-T* constraints on metamorphism and deformation in the Rapid River and Pollock Mountain plates and the age of displacement along the Pollock Mountain thrust fault, we propose that west-northwest–directed thrust faulting may have controlled loading and flattening deformation during the accretionary growth of the North American Cordillera. *P-T* paths require simultaneous loading of the Rapid River plate to 7–9 kbar at ~675 °C, exhumation and cooling of the Pollock Mountain plate, and deformation along the Pollock Mountain thrust fault that separates the two plates. This could be accomplished by thrust juxtaposition of the Pollock Mountain onto the Rapid River plate, resulting in loading and prograde metamorphism in the Rapid River plate. Timing constraints placing older metamorphic rocks on younger metamorphic rocks probably represents metamorphism associated with specific thrust loading events, which are not necessarily related to individual terrane collisions. This model highlights the role of localized deformation, including thrust faulting, in loading sedimentary basinal suites to amphibolite facies metamorphic conditions, during a prolonged orogenic process. Therefore, metamorphic age constraints may represent a localized structural development as part of regional tectonism. The resolution of these local features may be improved through the use of microsampling within metamorphic grain domains and/or use of multiple isotopic systems to date deformation and metamorphism.

ACKNOWLEDGMENTS

Partial financial support for this work was provided by National Science Foundation (NSF) grant EAR-0911681 to Schwartz and Stowell. Support for the Arizona LaserChron Laboratory is provided by NSF grant EAR-0732436. Essential upgrading of the University of Alabama JEOL 8600 electron probe microanalyzer was provided by NSF grant EAR-0744467. We acknowledge comments and discussions with Kenneth Johnson and John Watkinson and Doug Tinkham for providing thermodynamic data files for Theriak-Domino. Constructive reviews from Félix Gervais, Reed Lewis, Karen Lund, Sarah Roeske, and two anonymous reviewers greatly improved this manuscript.

REFERENCES CITED

Alexander, R.S., and Schwartz, J.J., 2009, Metasedimentary rocks in the Baker terrane, Blue Mountains Province, NE Oregon: Geological Society of America Abstracts with Programs, v. 41, no. 7, p. 294.

Aliberti, E.A., 1988, A structural, petrologic, and isotopic study of the Rapid River area and selected mafic complexes in the northwestern US: Implications for the evolution of an abrupt island arc-continent boundary [Ph.D. thesis]: Cambridge, Massachusetts, Harvard University, 160 p.

Armstrong, J.T., 1984, Quantitative analysis of silicate and oxide minerals: A reevaluation of ZAF corrections and proposal for new Bence-Albee coefficients, *in* Romig, A.D., Jr., and Goldstein, J.I., eds., Microbeam analysis—1984: San Francisco, California, San Francisco Press, p. 208–212.

Armstrong, R.L., Taubeneck, W.H., and Hales, P.O., 1977, Rb-Sr and K-Ar geochronology of Mesozoic granitic rocks and their Sr isotopic composition, Oregon, Washington, and Idaho: Geological Society of America Bulletin, v. 88, p. 397–411, doi:10.1130/0016-7606(1977)88<397:RAKGOM>2.0.CO;2.

Avé Lallemant, H.G., 1995, Pre-Cretaceous tectonic evolution of the Blue Mountains province, northeastern Oregon, *in* Vallier, T.L., and Brooks, H.C., eds., Geology of the Blue Mountains region of Oregon, Idaho, and Washington; petrology and tectonic evolution of pre-Tertiary rocks of the Blue Mountains region: U.S. Geological Survey Professional Paper 1438, p. 359–414.

Blake, D.E., 1991, Geology of the western Idaho suture zone in the Salmon River gorge, west-central Idaho [Ph.D. thesis]: Pullman, Washington State University, 288 p.

Blake, D.E., Gray, K.D., Giorgis, S., and Tikoff, B., 2009, A tectonic transect through the Salmon River suture zone along the Salmon River Canyon in the Riggins region of west-central Idaho, *in* O'Connor, J.E., et al., eds., Volcanoes to vineyards: Geologic field trips through the dynamic landscape of the Pacific Northwest: Geological Society of America Field Guide 15, p. 345–372, doi:10.1130/2009.fld015(18).

Blake, D.E., Bruce, M.L., and Reed, D.N., 2016, Geologic map of the Riggins Hot Springs quadrangle and adjacent areas, Idaho County, Idaho: Idaho Geological Survey Geologic Map 53, scale 1:24,000.

Bollen, E.M., 2015, Explaining discontinuous garnet zoning using reaction history P-T models: An example from the Salmon River suture zone, west-central Idaho [M.S. thesis]: Tuscaloosa, University of Alabama, 103 p.

Bosbyshell, H., Srogi, L., and Blackmer, G.C., 2016, Monazite age constraints on the tectonothermal evolution of the central Appalachian Piedmont: American Mineralogist, v. 101, p. 1820–1838, doi:10.2138/am-2016-5482.

Braudy, N., Gaschnig, R.M., Wilford, D., Vervoort, J.D., Nelson, C.L., Davidson, C., Kahn, M.J., and Tikoff, B., 2017, Timing and deformation conditions of the western Idaho shear zone, West Mountain, west-central Idaho: Lithosphere, v. 9, p. 157–183, doi:10.1130/L519.1.

Brooks, H.C., and Vallier, T.L., 1978, Mesozoic rocks and tectonic evolution of eastern Oregon and western Idaho, *in* Howell, D.G., and McDougall, K.A., eds., Mesozoic paleogeography of the western United States: Pacific Section, Society of Economic Paleontologists and Mineralogists, Pacific Coast Paleogeography Symposium 2, p. 146–188.

Bruce, M.L., 1998, Geology across the western boundary of the western Idaho suture zone, Lake Creek area, Riggins, Idaho [M.S. thesis]: Wilmington, University of North Carolina, 137 p.

Burchfield, B.C., Cowan, D., and Davis, G., 1992, Tectonic overview of the Cordilleran orogen in the western United States, *in* Burchfield, B.C., et al., eds., The Cordilleran orogen: Conterminous U.S.: Boulder, Colorado, Geological Society of America, Geology of North America v. G-3, p. 407–479, doi:10.1130/DNAG-GNA-G3.407.

Chamberlain, C.P., and Karabinos, P., 1987, Influence of deformation on pressure-temperature paths of metamorphism: Geology, v. 15, p. 42–44, doi:10.1130/0091-7613(1987)15<42:IODOPP>2.0.CO;2.

Chang, Z., Vervoort, J.D., Knaack, C., and McClelland, W.C., 2006, U-Pb dating of zircon by LA-ICP-MS: Geochemistry, Geophysics, Geosystems, v. 7, p. 1–14, Q05009, doi:10.1029/2005GC001100.

Coggon, R., and Holland, T.J.B., 2002, Mixing properties of phengitic micas and revised garnet-phengite thermobarometers: Journal of Metamorphic Geology, v. 20, p. 683–696, doi:10.1046/j.1525-1314.2002.00395.x.

Compston, W., Williams, I.S., and Meyer, C., 1984, U-Pb geochronology of zircons from lunar breccia 73217 using a sensitive high mass-resolution ion microprobe: Journal of Geophysical Research, v. 89, p. B525–B534, doi:10.1029/JB089iS02p0B525.

Coney, P.J., Jones, D.L., and Monger, J.W.H., 1980, Cordilleran suspect terranes: Nature, v. 288, p. 329–333, doi:10.1038/288329a0.

de Capitani, C., and Brown, T.H., 1987, The computation of chemical equilibrium in complex systems containing non-ideal solutions: Geochimica et Cosmochimica Acta, v. 51, p. 2639–2652, doi:10.1016/0016-7037(87)90145-1.

de Capitani, C., and Petrakakis, K., 2010, The computation of equilibrium assemblage diagrams with Theriak/Domino software: American Mineralogist, v. 95, p. 1006–1016, doi:10.2138/am.2010.3354.

Dickinson, W.R., 1979, Mesozoic forearc basin in central Oregon: Geology, v. 7, p. 166–170, doi:10.1130/0091-7613(1979)7<166:MFBICO>2.0.CO;2.

Diener, J.F.A., and Powell, R., 2007, Revised activity-composition models for clinopyroxene and amphibole: Journal of Metamorphic Geology, v. 25, p. 631–656, doi:10.1111/j.1525-1314.2007.00720.x.

Dorsey, R.J., and LaMaskin, T.A., 2007, Stratigraphic record of Triassic-Jurassic collisional tectonics in the Blue Mountains province, northeastern Oregon: American Journal of Science, v. 307, p. 1167–1193, doi:10.2475/10.2007.03.

Engebretson, D.C., Cox, A., and Gordon, R.G., 1985, Relative plate motions between oceanic and continental plates in the Pacific Basin: Geological Society of America Special Paper 206, 59 p., doi:10.1130/SPE206-p1.

Ferns, M.L., and Brooks, H.C., 1995, The Bourne and Greenhorn subterranes of the Baker terrane, northeastern Oregon: Implications for the evolution of the Blue Mountains island arc system, *in* Vallier, T.L., and Brooks, H.C., eds., Geology of the Blue Mountains region of Oregon, Idaho, and Washington: Petrology and tectonic evolution of pre-Tertiary rocks of the Blue Mountains region: U.S. Geological Survey Professional Paper 1438, p. 331–358.

Fleck, R.J., and Criss, R.E., 2004, Location, age, and tectonic significance of the western Idaho suture zone (WISZ): U.S. Geological Survey Open-File Report 2004-1039, 48 p.

Gaschnig, R.M., Vervoort, J.D., Lewis, R.S., and McClelland, W.C., 2010, Migrating magmatism in the northern US Cordillera in situ U-Pb geochronology of the Idaho batholith: Contributions to Mineralogy and Petrology, v. 159, p. 863–883, doi:10.1007/s00410-009-0459-5.

Gehrels, G.E., Valencia, V., and Ruiz, J., 2008, Enhanced precision, accuracy, efficiency, and spatial resolution of U-Pb ages by laser ablation-multicollector-inductively coupled plasma-mass spectrometry: Geochemistry, Geophysics, Geosystems, v. 9, Q03017, doi:10.1029/2007GC001805.

Getty, S.R., Selverstone, J., Wernicke, B.P., Jacobsen, S.B., Aliberti, E., and Lux, D.R., 1993, Sm-Nd dating of multiple garnet growth events in an arc-continent collision zone, northwestern U.S. Cordillera: Contributions to Mineralogy and Petrology, v. 115, p. 45–57, doi:10.1007/BF00712977.

Giorgis, S., and Tikoff, B., 2004, Constraints on kinematics and strain from feldspar porphyroclast populations, *in* Alsop, I., et al., eds., Flow processes in faults and shear zones: Geological Society of London Special Publication 224, p. 265–285, doi:10.1144/GSL.SP.2004.224.01.17.

Giorgis, S., Tikoff, B., and McClelland, W., 2005, Missing Idaho arc: Transpressional modification of the $^{87}Sr/^{86}Sr$ transition on the western edge of the Idaho batholith: Geology, v. 33, p. 469–472, doi:10.1130/G20911.1.

Giorgis, S., McClelland, W., Fayon, A., Singer, B., and Tikoff, B., 2008, Timing of deformation and exhumation in the western Idaho shear zone, McCall, Idaho: Geological Society of America Bulletin, v. 120, p. 1119–1133, doi:10.1130/B26291.1.

Gray, K.D., 2013, Structure of the arc-continent transition in the Riggins region of west-central Idaho—Strip maps and structural sections: Idaho Geological Survey Technical Report 13-1, scale 1:24,000.

Gray, K.D., and Oldow, J.S., 2005, Contrasting structural histories of the Salmon River belt and Wallowa terrane: Implications for terrane accretion in northeastern Oregon and west-central Idaho: Geological Society of America Bulletin, v. 117, p. 687–706, doi:10.1130/B25411.1.

Gray, K.D., Watkinson, A.J., Gaschnig, R.M., and Isakson, V.H., 2012, Age and structure of the Crevice pluton: Overlapping orogens in west-central Idaho?: Canadian Journal of Earth Sciences, v. 49, p. 709–731, doi:10.1139/e2012-016.

Hamilton, W., 1960, Metamorphism and thrust faulting in the Riggins quadrangle, Idaho, *in* Geological Survey Research 1960: U.S. Geological Survey Professional Paper 400-B, p. 230–231.

Hamilton, W., 1963, Metamorphism in the Riggins region, western Idaho: U.S. Geological Survey Professional Paper 436, 95 p.

Hamilton, W., 1969, Reconnaissance geologic map of the Riggins quadrangle, west-central Idaho: U.S. Geological Survey Map I-579, scale 1:25,000.

Hillhouse, J.W., Gromme, C.S., and Vallier, T.L., 1982, Paleomagnetism and Mesozoic tectonics of the Seven Devils volcanic arc in northeastern Oregon: Journal of Geophysical Research, v. 87, p. 3777–3794, doi:10.1029/JB087iB05p03777.

Holland, T.J.B., and Powell, R., 1998, An internally consistent thermodynamic data set for phases of petrological interest: Journal of Metamorphic Geology, v. 16, p. 309–343, doi:10.1111/j.1525-1314.1998.00140.x.

Holland, T.J.B., and Powell, R., 2000, AX, Mineral activity calculation for thermobarometry, Computer program AX2 version 2.2: Cambridge, Cambridge University Press.

Holland, T.J.B., and Powell, R., 2004, An internally consistent thermodynamic data set for phases of petrological interest: Journal of Metamorphic Geology, v. 16, p. 309–343, doi:10.1130/j.1525-1314.1998.00140.x.

Hodges, K.V., and Royden, L., 1984, Geologic thermobarometry of retrograded metamorphic rocks: An indication of the uplift trajectory of a portion of the northern Scandinavian Caledonides: Journal of Geophysical Research, v. 89, p. 7077–7090, doi:10.1029/JB089iB08p07077.

Hodges, K.V., and Spear, F.S., 1982, Geothermometry, geobarometry and the Al_2SiO_5 triple point at Mt. Moosilauke, New Hampshire: American Mineralogist, v. 67, p. 1118–1134.

Hyndman, R.D., Currie, C.A., and Mazzotti, S.P., 2005, Subduction zone backarcs, mobile belts, and orogenic heat: GSA Today, v. 15, no. 2, p. 4–10, doi:10.1130/1052-5173(2005)015<4:SZBMBA>2.0.CO;2.

Jeffcoat, R.C., Johnson, K., Schwartz, J.J., and Wooden, J.L., 2013, Petrogenesis of tonalitic-trondhjemitic magmas at mid- to lower-crustal depths in an arc-continent suture: A comparison of the geochronology, geobarometry, and geochemistry of the Deep Creek and Round Valley plutons, western Idaho: Geological Society of America Abstracts with Programs, v. 45, no. 3, p. 86.

Kauffman, J.D., Lewis, R.S., Schmidt, K.L., Stewart, D.E., Garwood, D.L., and Othberg, K.L., 2011, Geologic map of the Dairy Mountain Quadrangle, Idaho County, Idaho: Idaho Geological Survey Digital Web Map 129.

Kauffman, J.D., Schmidt, K.L., Lewis, R.S., Steward, D.E., Othberg, K.L., and Garwood, D.L., 2014, Geologic map of the Idaho part of the Grangeville 30 × 60 minute quadrangle, and adjoining areas of Washington and Oregon: Idaho Geological Survey Geologic Map 50, scale 1:100,000.

Kohn, M.J., and Spear, F.S., 1989, Empirical calibration of geobarometers for the assemblage garnet + plagioclase + quartz: American Mineralogist, v. 74, p. 77–84.

Koziol, A.M., and Newton, R.C., 1988, Redetermination of the anorthite breakdown reaction and improvement of the plagioclase-garnet-Al_2SiO_5-quartz geobarometer: American Mineralogist, v. 73, p. 216–223.

Kretz, R., 1983, Symbols for rock-forming minerals: American Mineralogist, v. 68, p. 277–279.

Kurz, G.A., Schmitz, M.D., Northrup, C.J., and Vallier, T.L., 2012, U-Pb geochronology and geochemistry of intrusive rocks from the Cougar Creek Complex, Wallowa arc terrane, Blue Mountains Province, Oregon-Idaho: Geological Society of America Bulletin, v. 124, p. 578–595, doi:10.1130/B30452.1.

LaMaskin, T.A., Dorsey, R.J., Vervoort, J.D., Schmitz, M.D., Tumpane, K.P., and Moore, N.O., 2015, Westward growth of Laurentia by pre-Late Jurassic terrane accretion, eastern Oregon and western Idaho, United States: Journal of Geology, v. 123, p. 233–267, doi:10.1086/681724.

Ludwig, K.R., 2003, User's Manual for Isoplot/Ex, Version 3.0, A geochronological toolkit for Microsoft Excel: Berkeley Geochronology Center Special Publication 4, 77 p.

Lund, K., 1984, Tectonic history of a continent-island arc boundary, west-central Idaho [Ph.D. thesis]: University Park, Pennsylvania State University, 210 p.

Lund, K., 2004, Geology of the Payette National Forest and vicinity, west-central Idaho: U.S. Geological Survey Professional Paper 1666, 89 p.

Lund, K., and Snee, L.W., 1988, Metamorphism, structural development, and age of the continent-island arc juncture in west-central Idaho, *in* Ernst, W.G., ed., Metamorphism and crustal evolution of the western United States: Englewood Cliffs, New Jersey, Prentice-Hall, p. 296–331.

Lund, K., McCollough, W.F., and Price, E.H., 1993, Geologic map of the Slate Creek–John Day Creek area, Idaho County, Idaho: U.S. Geological Survey Miscellaneous Investigation Map I-2299, scale 1:50,000.

Manduca, C.A., 1988, Geology and geochemistry of the ocean arc-continent boundary in the western Idaho batholith near McCall [Ph.D. thesis]: Pasadena, California Institute of Technology, 272 p.

Manduca, C.A., Kuntz, M.A., and Silver, L.T., 1993, Emplacement and deformation history of the western margin of the Idaho batholith near McCall, Idaho: Influence of a major terrane boundary: Geological Society of America Bulletin, v. 105, p. 749–765, doi:10.1130/0016-7606(1993)105<0749:EADHOT>2.3.CO;2.

McClelland, W.C., and Oldow, J.S., 2007, Late Cretaceous truncation of the western Idaho shear zone in the central North American Cordillera: Geology, v. 35, p. 723–726, doi:10.1130/G23623A.1.

McClelland, W.C., Tikoff, B., and Manduca, C.A., 2000, Two-phase evolution of accretionary margins: Examples from the North American Cordillera, *in* Housen, B., et al., eds., Advances in paleomagnetism and tectonics of active margins, in honor of the retirement of Myrl E. Beck, Jr.: Tectonophysics, v. 326, p. 37–55, doi:10.1016/S0040-1951(00)00145-1.

McKay, M.P., 2011, Pressure-temperature-time paths, prograde garnet growth, and protolith of tectonites from a polydeformational, polymetamorphic terrane: Salmon River suture zone, west-central Idaho [M.S. thesis]: Tuscaloosa, University of Alabama, 135 p.

Newton, R.C., and Haselton, H.T., 1981, Thermodynamics of the garnet-plagioclase-Al_2SiO_5-quartz geobarometer, *in* Newton, R.C., et al., eds., Thermodynamics of minerals and melts: New York, Springer, p. 131–147, doi:10.1007/978-1-4612-5871-1_8.

Oldow, J.S., Bally, A.W., Avé Lallemant, H.G., and Leeman, W.P., 1989, Phanerozoic evolution of the North American Cordillera: United States and Canada, *in* Bally, A.W., and Palmer, A.R., eds., The Geology of North America—An Overview: Boulder, Colorado, Geological Society of America, Geology of North America, v. A, p. 139–232, doi:10.1130/DNAG-GNA-A.139.

Onasch, C.M., 1977, Structural evolution of the western margin of the Idaho batholith in the Riggins, Idaho area [Ph.D. thesis]: University Park, Pennsylvania State University, 196 p.

Onasch, C.M., 1987, Temporal and spatial relations between folding, intrusion, metamorphism, and thrust folding in the Riggins area, west-central Idaho, *in* Vallier, T.L, and Brooks, H.C., eds., Geology of the Blue Mountains region of Oregon, Idaho, and Washington: The Idaho batholith and its border zone: U.S. Geological Survey Professional Paper 1436, p. 139–150.

Pollington, A.D., and Baxter, E.F., 2011, High precision microsampling and preparation of zoned garnet porphyroblasts for Sm-Nd geochronology: Chemical Geology, v. 281, p. 270–282, doi:10.1016/j.chemgeo.2010.12.014.

Powell, R., and Holland, T., 1994, Optimal geothermometry and geobarometry: American Mineralogist, v. 79, p. 120–133.

Powell, R., and Holland, T.J.B., 1999, Relating formulations of the thermodynamics of mineral solid solutions: Activity modeling of pyroxenes, amphiboles, and micas: American Mineralogist, v. 84, p. 1–14.

Prince, C.I., Kosler, J., Vance, D., and Günther, D., 2000, Comparison of laser ablation ICP-MS and isotope dilution REE analyses—Implications for Sm-Nd garnet geochronology: Chemical Geology, v. 168, p. 255–274, doi:10.1016/S0009-2541(00)00203-5.

Schmidt, K.L., Gray, K.D., Lewis, R.S., Steven, C.J., and Isakson, V.H., 2016, Mesozoic tectonics west of the accretionary boundary in west-central Idaho: A road log along U.S. Highway 95 between Moscow and New Meadows, Idaho, *in* Lewis, R.S., and Schmidt, K.L., eds., Exploring the geology of the inland northwest: Geological Society of America Field Guide 41, p. 175–209, doi:10.1130/2016.0041(06).

Scholl, D.W., Vallier, T.L., and Stevenson, A.J., 1986, Terrane accretion, production, and continental growth: A perspective based on the origin and tectonic fate of the Aleutian–Bering Sea region: Geology, v. 14, p. 43–47, doi:10.1130/0091-7613(1986)14<43:TAPACG>2.0.CO;2.

Schwartz, J.J., Snoke, A.W., Frost, C.D., Barnes, C.G., Gromet, L.P., and Johnson, K., 2010, Analysis of the Wallowa-Baker terrane boundary: Implications for tectonic accretion in the Blue Mountains Province, northeastern Oregon: Geological Society of America Bulletin, v. 122, p. 517–536, doi:10.1130/B26493.1.

Schwartz, J.J., Snoke, A.W., Cordley, F., Johnson, K., Frost, C.D., Barnes, C.G., LaMaskin, T.A., and Wooden, J.L., 2011, Late Jurassic magmatism, metamorphism, and deformation in the Blue Mountains Province, northeastern Oregon: Geological Society of America Bulletin, v. 123, p. 2083–2111, doi:10.1130/B30327.1.

Schwartz, J.J., Johnson, K., Mueller, P., Valley, J., Strickland, A., and Wooden, J.L., 2014, Time scales and processes of Cordilleran batholith construction and high-Sr/Y magmatic pulses: Evidence from the Bald Mountain batholith, northeastern Oregon: Geosphere, v. 10, p. 1456–1481, doi:10.1130/GES01033.1.

Selverstone, J., Wernicke, B.P., and Aliberti, E.A., 1992, Intracontinental subduction and hinged unroofing along the SRSZ, west-central Idaho: Tectonics, v. 11, p. 124–144, doi:10.1029/91TC02418.

Silberling, N.J., Jones, D.L., Blake, M.C., Jr., and Howell, D.G., 1984, Lithotectonic terrane map of the western conterminous United States, *in* Silberling, N.J., and Jones, D.L., eds., Lithotectonic terrane maps of the North American Cordillera: U.S. Geological Survey Open-File Report 84-523, 43 p.

Silberling, N.J., Jones, D.L., Blake, M.C., Jr., and Howell, D.G., 1987, Lithotectonic terrane map of the western conterminous United States: U.S. Geological Survey Miscellaneous Field Studies Map 1874-C, scale 1:2,500,000.

Snee, L.W., Lund, K., Sutter, J.F., Balcer, D.E., and Evans, K.V., 1995, An $^{40}Ar/^{39}Ar$ chronicle of the tectonic development of the Salmon River suture zone, western Idaho, *in* Vallier, T.L., and Brooks, H.C., eds., Geology of the Blue Mountains region of Oregon, Idaho, and Washington; petrology and tectonic evolution of pre-Tertiary rocks of the Blue Mountains region: U.S. Geological Survey Professional Paper 1438, p. 359–414.

Spear, F.S., 1993, Metamorphic phase equilibria and pressure-temperature-time paths: Mineralogical Society of America Monograph 1, 799 p.

Spear, F.S., Hickmott, D.D., and Selverstone, J., 1990, Metamorphic consequences of thrust emplacement, Fall Mountain, New Hampshire: Geological Society of America Bulletin, v. 102, p. 1344–1360, doi:10.1130/0016-7606(1990)102<1344:MCOTEF>2.3.CO;2.

Spencer, K.J., Hacker, B.R., Kylander-Clark, A.R.C., Andersen, T.B., Cottle, J.M., Stearns, M.A., Poletti, J.E., and Seward, G.G.E., 2013, Campaign-style titanite U-Pb dating by laser-ablation ICP: Implications for crustal flow, phase transformations and titanite closure: Chemical Geology, v. 341, p. 84–101, doi:10.1016/j.chemgeo.2012.11.012.

Stearns, M.A., Hacker, B.R., Ratschbacher, L., Rutte, D., and Kylander-Clark, A.R.C., 2015, Titanite petrochronology of the Pamir gneiss domes: Implications for mid-deep crust exhumation and titanite closure to Pb and Zr diffusion: Tectonics, v. 34, p. 784–802, doi:10.1002/2014TC003774.

Stern, R.J., 2002, Subduction zones: Reviews of Geophysics, v. 40, p. 3-1–3-38, doi:10.1029/2001RG000105.

Stowell, H.H., and Goldberg, S.A., 1997, Sm-Nd garnet dating of polyphase metamorphism: northern Coast Mountains, southeastern Alaska: Journal of Metamorphic Geology, v. 15, p. 439–450, doi:10.1111/j.1525-1314.1997.00025.x.

Stowell, H.H., and Tinkham, D.K., 2003, Integration of phase equilibria modeling and garnet Sm-Nd chronology for construction of P-T-t paths: Examples from the Cordilleran Coast Plutonic Complex, USA, *in* Vance, D., et al., eds., Geochronology: Linking the isotopic record with petrology and textures: Geological Society of London Special Publication 220, p. 119–145, doi:10.1144/GSL.SP.2003.220.01.07.

Stowell, H.H., Tullock, A., Zuluaga, C.A., and Koenig, A., 2010, Timing and duration of garnet granulite metamorphism in magmatic arc crust, Fiordland, New Zealand: Chemical Geology, v. 273, p. 91–110, doi:10.1016/j.chemgeo.2010.02.015.

Taubeneck, W.H., 1971, Idaho batholith and its southern extension: Geological Society of America Bulletin, v. 82, p. 1899–1928, doi:10.1130/0016-7606(1971)82[1899:IBAISE]2.0.CO;2.

Tikoff, B., Kelso, P., Manduca, C.A., Markley, M.J., and Gillaspy, J., 2001, Lithospheric and crustal reactivation of an ancient plate boundary: The assembly and disassembly of the Salmon River suture zone, Idaho, USA: Geological Society, London, Special Publications, v. 186, p. 213–231, doi:10.1144/GSL.SP.2001.186.01.13.

Tinkham, D.K., Zuluaga, C.A., and Stowell, H.H., 2001, Metapelitic phase equilibria modeling in MnNCKFMASH: The effect of variable Al_2O_3 and MgO/(MgO+FeO) on mineral stability: Geological Materials Research, v. 3, p. 1–42.

Unruh, D.M., Lund, K., Kuntz, M.A., and Snee, S.W., 2008, Uranium-lead zircon ages and Sr, Nd, and Pb isotope geochemistry of selected plutonic rocks from western Idaho: U.S. Geological Survey Open-File Report 2008-1142, 24 p.

Vallier, T.L., 1977, The Permian and Triassic Seven Devils Group, western Idaho and northeastern Oregon: U.S. Geological Survey Bulletin, v. 1437, p. 58.

Vallier, T.L., 1995, Petrology of pre-Tertiary igneous rocks in the Blue Mountains region of Oregon, Idaho, and Washington: Implications for the geologic evolution of a complex island arc, *in* Vallier, T.L., and Brooks, H.C., eds., Geology of the Blue Mountains region of Oregon, Idaho, and Washington: U.S. Geological Survey Professional Paper 1438, p. 125–209.

Vallier, T.L., 1998, Islands and Rapids: A Geologic Story of Hells Canyon: Lewiston, Idaho, Confluence Press, 151 p.

van Staal, C.R., Currie, K.L., Rowbotham, G., Goodfellow, W., and Rogers, N., 2008, Pressure-temperature paths and exhumation of Late Ordovician–Early Silurian blueschists and associated metamorphic nappes of the Salinic Brunswick subduction complex, northern Appalachians: Geological Society of America Bulletin, v. 120, p. 1455–1477, doi:10.1130/B26324.1.

Vavra, G., Schmid, R., and Gebauer, D., 1999, Internal morphology, habit and U-Th-Pb microanalysis of amphibolite-to-granulite facies zircons: Geochronology of the Ivrea Zone (Southern Alps): Contributions to Mineralogy and Petrology, v. 134, p. 380–404, doi:10.1007/s004100050492.

Walker, N.W., 1986, U-Pb geochronologic and petrologic studies in the Blue Mountains terranes, northeastern Oregon and westernmost-central Idaho—Implications for pre-Tertiary tectonic evolution [Ph.D. thesis]: University of California Santa Barbara, 224 p.

Watanabe, T., Langseth, M.G., and Anderson, R.N., 2013, Heat flow in back-arc basins of the western Pacific, *in* Talwani, M., and Pitman, W.C., eds., Island arcs, deep sea trenches and back-arc basins: Maurice Ewing Series, Volume 1: Washington, D.C., American Geophysical Union, p. 137–161, doi:10.1029/ME001p0137.

White, R.W., Powell, R., and Clarke, G.L., 2002, The interpretation of reaction textures in Fe-rich metapelitic granulites of the Musgrave block, central Australia: Constraints from mineral equilibria calculations in the system K_2O-FeO-MgO-Al_2O_3-SiO_2-H_2O-TiO_2-Fe_2O_3: Journal of Metamorphic Geology, v. 20, p. 41–55, doi:10.1046/j.0263-4929.2001.00349.x.

White, R.W., Pomroy, N.E., and Powell, R., 2005, An in-situ metatexite-diatexite transition in upper amphibolite facies rocks from Broken Hill, Australia: Journal of Metamorphic Geology, v. 23, p. 579–602, doi:10.1111/j.1525-1314.2005.00597.x.

White, R.W., Powell, R., and Holland, T.J.B., 2007, Progress relating to calculation of partial melting equilibria for metapelites: Journal of Metamorphic Geology, v. 25, p. 511–527, doi:10.1111/j.1525-1314.2007.00711.x.

Wilford, D., 2012, Lu-Hf geochronology of the Salmon River suture zone, west-central Idaho [M.S. thesis]: Pullman, Washington State University, 97 p.

Williams, P.F., and Jiang, D., 1999, Rotating garnets: Journal of Metamorphic Geology, v. 17, p. 367–378, doi:10.1046/j.1525-1314.1999.00203.x.

Wilson, D., and Cox, A., 1980, Paleomagnetic evidence for tectonic rotation of Jurassic plutons in the Blue Mountains, eastern Oregon: Journal of Geophysical Research, v. 85, p. 3681–3689, doi:10.1029/JB085iB07p03681.

Wyld, S.J., and Wright, J.E., 2001, New evidence for Cretaceous strike-slip faulting in the United States Cordillera and implications for terrane displacement, deformation patterns, and plutonism: American Journal of Science, v. 301, p. 150–181, doi:10.2475/ajs.301.2.150.

Wyld, S.J., Umhoefer, P.J., and Wright, J.E., 2006, Reconstructing northern Cordilleran terranes along known Cretaceous and Cenozoic strike-slip faults: Implications for the Baja British Columbia hypothesis and other models, *in* Haggart, J.W., et al., eds., Paleogeography of the North American Cordillera: Evidence for and against large-scale displacements: Geological Association of Canada Special Paper 46, p. 277–298.

Žák, J., Verner, K., Tomek, F., Holub, F.V., Johnson, K., and Schwartz, J.J., 2015, Simultaneous batholith emplacement, terrane/continent collision, and oroclinal bending in the Blue Mountains Province, North American Cordillera: Tectonics, v. 34, p. 1107–1128, doi:10.1002/2015TC003859.

Zen, E., and Hammarstrom, J.M., 1984, Magmatic epidote and its petrologic significance: Geology, v. 12, p. 515–518, doi:10.1130/0091-7613(1984)12<515:MEAIPS>2.0.CO;2.

MANUSCRIPT RECEIVED 28 DECEMBER 2016
REVISED MANUSCRIPT RECEIVED 27 MARCH 2017
MANUSCRIPT ACCEPTED 2 MAY 2017

Printed in the USA